Journal of Computational Physics 229 (2010) 1514–1535

Contents lists available at ScienceDirect

Journal of Computational Physics

journal homepage: www.elsevier.com/locate/jcp

The constrained reinitialization equation for level set methods

Daniel Hartmann *, Matthias Meinke, Wolfgang Schröder

Institute of Aerodynamics, RWTH Aachen University, Wüllnerstr. 5a, 52062 Aachen, Germany

ARTICLE INFO

Article history:
Received 19 January 2009
Received in revised form 12 August 2009
Accepted 26 October 2009
Available online 3 November 2009

Keywords:
Level set method
Reinitialization
Distance function
Eikonal equation

ABSTRACT

Based on the constrained reinitialization scheme [D. Hartmann, M. Meinke, W. Schröder, Differential equation based constrained reinitialization for level set methods, J. Comput. Phys. 227 (2008) 6821–6845] a new constrained reinitialization equation incorporating a forcing term is introduced. Two formulations for high-order constrained reinitialization (HCR) are presented combining the simplicity and generality of the original reinitialization equation [M. Sussman, P. Smereka, S. Osher, A level set approach for computing solutions to incompressible two-phase flow, J. Comput. Phys. 114 (1994) 146–159] in terms of high-order standard discretization and the accuracy of the constrained reinitialization scheme in terms of interface displacement. The novel HCR schemes represent simple extensions of standard implementations of the original reinitialization equation. The results evidence the significantly increased accuracy and robustness of the novel schemes.

1. Introduction

From their inception [1], level set methods have been established in many areas of and beyond computational physics to capture the motion of interfaces. This interface motion is in level set methods represented by an evolving scalar field. It is one of the great challenges of level set methods, however, that the scalar field often has to be frequently regularized to accurately compute discrete derivatives needed to evolve the field. Usually, the scalar field is initialized into a signed distance function and a reinitialization is performed to regularize the field. Other techniques to increase the fidelity of the level set method include the particle level set method introduced in [2] and coupled volume-of-fluid/level set methods discussed in [3,4], where the level set function is corrected using Lagrangian particles or the mass-conservation property of the volume-of-fluid method, respectively. Further methods rely on increased grid resolution using either adaptive mesh refinement as employed in [5] or a separately refined mesh for the level set method [6,7].

To reinitialize the level set field, a partial differential equation, which can be iteratively solved to transform an arbitrary scalar field into a signed distance function, is proposed in [8]. However, using this partial differential equation for the reinitialization is known to change the level set solution [9–11]. To be more precise, discretely solving this equation results in a significant displacement of the interface location, i.e., the interface is unphysically shifted during the reinitialization process. Modifications of the original formulation addressing this problem are proposed in [10,11,5] and more recently in [9], where the constrained reinitialization (CR) scheme is derived taking the location of the interface explicitly into account. The resulting CR scheme provides explicit equations to compute the signed distance function on the discrete computational points directly at the front, while away from the front the original reinitialization equation can be used. The method is second-order accurate in the location of the front and significantly reduces the displacement of the interface [9,12].

In this paper, the CR approach of Hartmann et al. [9] is generalized to higher-order schemes. Based on the expressions derived in [9], an explicit forcing term is formulated and introduced into the original reinitialization equation. This allows

* Corresponding author. Tel.: +49 241 80 90396; fax: +49 241 80 92257.
E-mail address: office@aia.rwth-aachen.de (D. Hartmann).

0021-9991/$ - see front matter © 2009 Elsevier Inc. All rights reserved.
doi:10.1016/j.jcp.2009.10.042

the reinitialization equation to be discretized with arbitrarily high-order schemes, while the forcing term acts as a constraint fixing the location of the interface.

The structure of the paper is as follows. After a brief introduction of the level set method in Section 2 and the reinitialization procedure in Section 3, the novel constrained reinitialization equation is introduced in Section 4. Results of two-and three-dimensional computations are given in Section 5, before the findings of the present paper are summarized in Section 6.

2. Level set transport

Consider an interface defined by

$$\phi_0 = \{(\mathbf{x}, t) : \phi(\mathbf{x}, t) = 0\}, \quad \mathbf{x} \in R^n, \ t \in R^+, \tag{1}$$

where $\phi(\mathbf{x}, t)$ is the scalar level set function. For $n = 3$, let the components of the coordinate vector be denoted by $\mathbf{x} = (x, y, z)^T$. The level set function ϕ is specified as a signed distance function with respect to ϕ_0 with the properties

$$\begin{cases} \phi > 0 & \text{for } \mathbf{x} \in \Omega^+, \\ \phi = 0 & \text{for } \mathbf{x} \in \phi_0, \\ \phi < 0 & \text{for } \mathbf{x} \in \Omega^-, \end{cases} \tag{2}$$

where the computational domain Ω has been decomposed, $\Omega = \{\Omega^+, \Omega^-, \phi_0\}$, with $\Omega^+ \cap \Omega^- = \emptyset$ and $\phi_0 \notin \{\Omega^+, \Omega^-\}$. The level set equation governing the evolution of ϕ in Ω can be formulated

$$\partial_t \phi + \mathbf{f} \cdot \nabla \phi = 0, \tag{3}$$

where $\mathbf{f} = \mathbf{f}(\mathbf{x}, t)$ is the extension velocity vector describing the motion of the local level set. A great advantage of level set methods is that geometric quantities such as the normal vector $\mathbf{n}$ and the curvature $\mathfrak{C}$ can be readily obtained from the scalar level set field

$$\mathbf{n} = -\frac{\nabla \phi}{|\nabla \phi|}, \tag{4a}$$

$$\mathfrak{C} = \nabla \cdot \mathbf{n}, \tag{4b}$$

where the normal vector $\mathbf{n}$ is defined such that it points into Ω^-.

3. Reinitialization

As noted in the introduction, the level set function ϕ is usually initialized into a signed distance function, which is the unique viscosity solution of the Eikonal equation

$$|\nabla \phi| = 1, \tag{5}$$

with the boundary condition $\phi = \phi_0$ at the interface. However, once initialized into such a signed distance function, the level set function ϕ usually does not retain this property under the evolution of Eq. (3) and needs to be reinitialized at regular time intervals [9,10,12]. Sussman et al. [8] reformulate the Eikonal equation (5) as an evolution equation in artificial time τ

$$\partial_\tau \phi^v + S(\tilde{\phi})(|\nabla \phi^v| - 1) = 0, \tag{6}$$

where the superscript ^{v} denotes the discrete pseudo-time step level. The quantity $S(\tilde{\phi})$ is a smoothed sign function of the perturbed level set function $\tilde{\phi} = \tilde{\phi}(\mathbf{x}, \tau = 0)$ being defined as

$$S(\tilde{\phi}) = \frac{\tilde{\phi}}{\sqrt{\tilde{\phi}^2 + \epsilon^2}}, \tag{7}$$

where ϵ is a smoothing parameter and is usually chosen equal to the grid spacing $\epsilon = h$ [8]. A modified smoothed sign function to achieve faster convergence in regions where $|\nabla \phi|$ is small is proposed by Peng et al. [10] and can be substituted for Eq. (7).

Analytically, Eq. (6) transforms an arbitrary scalar field ϕ into a signed distance function d with respect to the interface ϕ_0. However, when Eq. (6) is solved on a discrete grid the interface is significantly displaced during the reinitialization procedure [9,12]. The constrained reinitialization (CR) scheme developed recently by Hartmann et al. [9] addresses this problem by explicitly taking into account the location of the interface during the reinitialization process. The resulting expressions are explicit equations for the signed distance function on the cells at the interface, while on all other cells away from the interface Eq. (6) can be solved. For efficiency, a standard first-order upwind spatial discretization is used for Eq. (6) [9]. In [12], the novel scheme is compared against the standard reinitialization Eq. (6) spatially discretized with a first-order upwind and a fifth-order Hamilton–Jacobi WENO scheme [13]. The results show the CR scheme to be significantly superior

to the other investigated schemes for a simple propagation test case. For the CR scheme, the displacement caused during the reinitialization procedure is found to be approximately an order of magnitude smaller than for the fifth-order WENO standard reinitialization and roughly three orders of magnitude smaller than for the first-order upwind standard reinitialization.

To generalize the CR scheme to arbitrarily high-order discretization schemes, a new reinitialization equation denoted the constrained reinitialization equation is proposed in the following. The resulting high-order constrained reinitialization (HCR) schemes are based on the expressions derived for the CR scheme and can be easily implemented as an extension of the original reinitialization Eq. (6).

4. High-order constrained reinitialization

We begin by briefly reviewing the two formulations CR-1 and CR-2 of the CR scheme. Then, the fundamental constrained reinitialization formulation is rewritten to obtain a forcing term which can be introduced into the original reinitialization equation to give the new constrained reinitialization equation, which is the basis of high-order constrained reinitialization (HCR).

4.1. Recap of CR-1 and CR-2

On a three-dimensional structured grid with a uniform spacing Δx, consider a cell located at $\mathbf{x}_{i,j,k}$ with $\tilde{\phi}_{i,j,k} < 0$ and two cells at $\mathbf{x}_{i+1,j,k}$ and at $\mathbf{x}_{i,j+1,k}$ with $\tilde{\phi}_{i+1,j,k} > 0$ and $\tilde{\phi}_{i,j+1,k} > 0$, respectively, where $\tilde{\phi}$ denotes the value of ϕ before the reinitialization. That is, by linear interpolation between the cells one can determine two interface locations

$$\begin{cases} \mathbf{x}_{i+\tilde{\theta}_1,j,k} \in \left[\mathbf{x}_{i,j,k}; \mathbf{x}_{i+1,j,k}\right], \\ \mathbf{x}_{i,j+\tilde{\theta}_2,k} \in \left[\mathbf{x}_{i,j,k}; \mathbf{x}_{i,j+1,k}\right], \end{cases} \tag{8a}$$

where

$$\begin{cases} \tilde{\theta}_1 = \frac{\tilde{\phi}_{i,j,k}}{\tilde{\phi}_{i+1,j,k} - \tilde{\phi}_{i,j,k}}, \\ \tilde{\theta}_2 = \frac{\tilde{\phi}_{i,j,k}}{\tilde{\phi}_{i,j+1,k} - \tilde{\phi}_{i,j,k}}, \end{cases} \tag{8b}$$

and $0 < \tilde{\theta}_{1,2} < 1$. After the reinitialization, linear interpolation yields the two locations

$$\begin{cases} \mathbf{x}_{i+\theta_1,j,k} \in \left[\mathbf{x}_{i,j,k}; \mathbf{x}_{i+1,j,k}\right], \\ \mathbf{x}_{i,j+\theta_2,k} \in \left[\mathbf{x}_{i,j,k}; \mathbf{x}_{i,j+1,k}\right], \end{cases} \tag{8c}$$

where

$$\begin{cases} \theta_1 = \frac{\phi_{i,j,k}}{\phi_{i+1,j,k} - \phi_{i,j,k}}, \\ \theta_2 = \frac{\phi_{i,j,k}}{\phi_{i,j+1,k} - \phi_{i,j,k}}, \end{cases} \tag{8d}$$

and in general $\theta_{1,2} \neq \tilde{\theta}_{1,2}$, such that the interface is displaced. This interface displacement is illustrated in Fig. 2. Assuming the signed distance function d is known at $\mathbf{x}_{i+1,j,k}$ and $\mathbf{x}_{i,j+1,k}$, a least-squares function is formulated to determine $\phi_{i,j,k}$ from the constraints $|\nabla\phi|_{i,j,k} = 1$ and $\tilde{\theta} = \theta$ for all discrete interface locations, which in general results in an overdetermined problem. Solving the least-squares problem is equivalent to minimizing the squared deviations from the constraints. This yields for the CR-1 formulation an explicit expression to approximate the signed distance $\tilde{d}_{i,j,k}$ at $\mathbf{x}_{i,j,k}$ [9]

$$\tilde{d}_{i,j,k} = \frac{\tilde{\phi}_{i,j,k}}{M_{i,j,k}} \sum_{\alpha=1}^{M_{i,j,k}} \frac{d_{(i,j,k)_\alpha}}{\tilde{\phi}_{(i,j,k)_\alpha}}. \tag{9}$$

The right-hand side of Eq. (9) depends on the signed distance function d and $\tilde{\phi}$ on the neighbor cells across the interface. These neighbor cells are denoted by the index $(i,j,k)_\alpha$ and collected in a set $\mathcal{S}_{i,j,k}$ defined

$$\mathcal{S}_{i,j,k} = \left\{\mathbf{x}_{(i,j,k)_\alpha} : \phi_{i,j,k}\phi_{(i,j,k)_\alpha} < 0\right\}. \tag{10}$$

In the example above $(i,j,k)_1 = (i+1,j,k)$ and $(i,j,k)_2 = (i,j+1,k)$. The quantity $M_{i,j,k}$ is the number of such neighbors, i.e., $M_{i,j,k} = 2$ in the present example. The signed distance functions $d_{i+1,j,k}$ and $d_{i,j+1,k}$ on the cells across the interface are computed by an explicit formula [9]. For a cell at $\mathbf{x}_{i,j,k}$ the function reads

$$d_{i,j,k} = \frac{\tilde{\phi}_{i,j,k}}{\left(\left[\partial_x\tilde{\phi}_{i,j,k}\right]^2 + \left[\partial_y\tilde{\phi}_{i,j,k}\right]^2 + \left[\partial_z\tilde{\phi}_{i,j,k}\right]^2\right)^{1/2}}. \tag{11}$$

A suitable discretization of the derivatives $[\partial_\zeta\tilde{\phi}_{i,j,k}]$, $\zeta = \{x,y,z\}$, in Eq. (11) is given in [9].

The formulation CR-2 is derived by reducing the number of constraints imposed on the scheme CR-1. A determined problem is obtained such that the location of the interface can be preserved throughout the reinitialization. Instead of minimizing the interface displacement at all locations which can be identified by linear interpolation between neighbor cells, the interface location is only fixed at one point representative of these locations. Formally, this point is determined by averaging the interface coordinates obtained by linear interpolation. As for CR-1, an explicit determining equation for the signed distance $\tilde{d}_{i,j,k}$ at $\mathbf{x}_{i,j,k}$ is obtained [9]

$$\tilde{d}_{i,j,k} = \tilde{\phi}_{i,j,k} \sum_{\alpha=1}^{M_{i,j,k}} d_{(i,j,k)_\alpha} \left(\sum_{\alpha=1}^{M_{i,j,k}} \tilde{\phi}_{(i,j,k)_\alpha} \right)^{-1}, \tag{12}$$

with the same notation as in Eq. (9).

What remains to be done is to determine on which cells Eqs. (9) or (12) are used to determine the signed distance function. Let Γ be defined as the set of cells identified by their coordinate vector which are adjacent to the zero level set

$$\Gamma = \left\{ \mathbf{x}_{i,j,k} : \left(\Pi^{i,j,k}_{i',j,k} \phi \leqslant 0 \right) \vee \left(\Pi^{i,j,k}_{i,j',k} \phi \leqslant 0 \right) \vee \left(\Pi^{i,j,k}_{i,j,k'} \phi \leqslant 0 \right) \right\} \tag{13}$$

for any combination of integers $i' \in \{i+1, i-1\}, j' \in \{j+1, j-1\}, k' \in \{k+1, k-1\}$ with $\Pi^{i,j,k}_{i',j,k} \phi = \phi_{i,j,k} \phi_{i',j,k}$. That is, all cells in Γ are located within a distance Δx from the zero level set. According to [12], the signed distance function d is computed first on all these cells in Γ. Afterwards, the signed distance function is updated on a subset of cells $\mathcal{C} \subset \Gamma$ via Eqs. (9) or (12), depending on whether CR-1 or CR-2 is used, where $\mathcal{C}$ is defined [9,14]

$$\mathcal{C} = \left\{ \mathbf{x}_{i,j,k} \in \Gamma : \mathfrak{C}_{i,j,k} \tilde{\phi}_{i,j,k} < 0 \vee (\mathfrak{C}_{i,j,k} = 0 \wedge \tilde{\phi}_{i,j,k} < 0) \right\}, \tag{14}$$

and $\mathfrak{C}_{i,j,k}$ denotes the discretely approximated curvature at $\mathbf{x}_{i,j,k}$. The curvature $\mathfrak{C}_{i,j,k}$ is approximated using centered differences for the divergence of the normal vector.

4.2. Formulation of HCR-1 and HCR-2

The key idea to generalize the CR scheme is to replace the explicit expressions for the signed distance function d and $\tilde{d}$ by a forcing term which can be introduced into the original reinitialization Eq. (6), such that standard high-order spatial discretization schemes for this type of equation can be used. Introducing the forcing term $F^v = F(\phi^v, \mathbf{x})$, the new constrained reinitialization equation reads

$$\partial_\tau \phi^v + S(\tilde{\phi})(|\nabla \phi^v| - 1) = \beta F^v, \tag{15}$$

where β is a weighting factor which is set $\beta = 0.5$ in the present work. The reason for $\beta = 0.5$ is discussed below. Eq. (15) is solved on all cells in the computational domain.

To formulate the forcing term, assume the approximation of the signed distance function d on Γ to be given by the instantaneous solution ϕ^v at the iteration step v of (6), i.e., the signed distance function $d_{(i,j,k)_\alpha}$ required in Eqs. (9) and (12) is replaced by $\phi^v_{(i,j,k)_\alpha}$. Recasting Eqs. (9) and (12) accordingly yields the expressions

$$\psi^v_{i,j,k} = \frac{1}{M_{i,j,k}} \sum_{\alpha=1}^{M_{i,j,k}} \frac{\tilde{\phi}_{i,j,k}}{\tilde{\phi}_{(i,j,k)_\alpha}} \phi^v_{(i,j,k)_\alpha}, \tag{16a}$$

$$\psi^v_{i,j,k} = \tilde{\phi}_{i,j,k} \sum_{\alpha=1}^{M_{i,j,k}} \phi^v_{(i,j,k)_\alpha} \left(\sum_{\alpha=1}^{M_{i,j,k}} \tilde{\phi}_{(i,j,k)_\alpha} \right)^{-1}, \tag{16b}$$

where ψ^v has been substituted for $\tilde{d}$. The quantity ψ^v represents a target value for the level set function ϕ at the iteration step v, which is determined such that the displacement of the interface during the reinitialization is corrected. It is computed based on the instantaneous level set solution ϕ^v during the reinitialization.

The forcing term F^v is formulated to drive the level set function towards this target value ψ^v on a subspace $\mathcal{C}^v \subseteq \Gamma$ to be defined below. On the cells in $\Gamma \setminus \mathcal{C}^v$ and those which are not at the interface, the original reinitialization remains unchanged and the forcing term F^v vanishes. Summarizing, on a discrete grid F^v can be decomposed into

$$F(\phi^v, \mathbf{x}_{i,j,k}) = \delta^{\mathcal{F}}_{i,j,k} \mathcal{F}^v_{i,j,k}, \tag{17a}$$

where the delta function is defined

$$\delta^{\mathcal{F}}_{i,j,k} = \begin{cases} 1 & \text{if } \mathbf{x}_{i,j,k} \in \mathcal{C}^v, \\ 0 & \text{otherwise}, \end{cases} \tag{17b}$$

and the discrete forcing term $\mathcal{F}^v_{i,j,k}$ is formulated

$$\mathcal{F}^v_{i,j,k} = \frac{1}{\Delta x} \left(\psi^v_{i,j,k} - \phi^v_{i,j,k} \right). \tag{17c}$$

On the right-hand side, the factor $1/\Delta x$ has been introduced to compensate the length scale inherent in $(\psi^v_{i,j,k} - \phi^v_{i,j,k})$, which scales with Δx.

The formulation (16) may become unstable when the level set function on a cell at $\mathbf{x}_{(i,j,k)_\alpha}$ changes the sign during the reinitialization such that $\phi^v_{(i,j,k)_\alpha}\phi^v_{i,j,k} > 0$ at some pseudo-time level v. For example, assume all $\phi^v_{(i,j,k)_\alpha}, \alpha = \{1,\dots,M_{i,j,k}\}$, change the sign from iteration step $v-1$ to step v since the interface has moved across these cells due to the reinitialization. Further, assume $\phi^v_{i,j,k}$ still has the correct sign, i.e., there is no other interface which has moved across this cell. Then, it can be seen from Eq. (16) that the target value also changes the sign, i.e., $\psi^{v-1}_{i,j,k}\psi^v_{i,j,k} < 0$ and $\psi^v_{i,j,k}\phi^v_{i,j,k} < 0$, such that a sign change of the level set function at $\mathbf{x}_{i,j,k}$ is incorrectly enforced. Even if only one of the cells at $\mathbf{x}_{(i,j,k)_\alpha}, \alpha \in \{1,\dots,M_{i,j,k}\}$, changes the sign its contribution in Eq. (16) becomes false. If this occurs for a cell at $\mathbf{x}_{i,j,k}$ at a pseudo-time level v the forcing is locally not applied on this particular cell and at this particular pseudo-time level v to avoid instabilities.

To this end, the subspace $\mathcal{C}^v \subseteq \Gamma$ used in Eq. (17b) is introduced

$$\mathcal{C}^v = \left\{\mathbf{x}_{i,j,k} \in \Gamma : \phi^v_{i,j,k}\phi^v_{(i,j,k)_\alpha} < 0 \ \forall \alpha \in \{1,\dots,M_{i,j,k}\}\right\}. \tag{18}$$

It contains all cells to which a forcing is applied and is updated at each pseudo-time level v. In the numerical experiments which are presented in Section 5 the discussed situation rarely occurs, such that in most cases $\mathcal{C}^v = \Gamma$. Only in the presented three-dimensional interface coalescing problem the sign of the level set function sporadically changes on a few cells during the reinitialization, such that the overall effect of the locally reduced forcing is negligible. Note, sign changes of $\phi_{i,j,k}$ do not raise a problem since the forcing term retains the correct sign.

Eqs. (16a) and (16b) correspond to the CR-1 and CR-2 formulation, respectively, and can be rewritten by introducing the expressions

$$r^{i,j,k}_{(i,j,k)_\alpha} = \tilde{\phi}_{i,j,k}\left(\tilde{\phi}_{(i,j,k)_\alpha}\right)^{-1}, \tag{19a}$$

$$\tilde{r}^{i,j,k} = \tilde{\phi}_{i,j,k}\left(\sum_{\alpha=1}^{M_{i,j,k}} \tilde{\phi}_{(i,j,k)_\alpha}\right)^{-1}, \tag{19b}$$

to obtain

$$\psi^v_{i,j,k} = \frac{1}{M_{i,j,k}} \sum_{\alpha=1}^{M_{i,j,k}} r^{i,j,k}_{(i,j,k)_\alpha}\phi^v_{(i,j,k)_\alpha}, \tag{20a}$$

$$\psi^v_{i,j,k} = \tilde{r}^{i,j,k} \sum_{\alpha=1}^{M_{i,j,k}} \phi^v_{(i,j,k)_\alpha}. \tag{20b}$$

Since $r^{i,j,k}_{(i,j,k)_\alpha}$ and $\tilde{r}^{i,j,k}$ only depend on the discrete values of the level set function before the reinitialization procedure, they can be computed as constants prior to the reinitialization. Eqs. (20a) and (20b) can be substituted into Eq. (17) to obtain the formulations HCR-1

$$\mathcal{F}^v_{i,j,k} = \frac{1}{\Delta x}\left(\frac{1}{M_{i,j,k}} \sum_{\alpha=1}^{M_{i,j,k}} r^{i,j,k}_{(i,j,k)_\alpha}\phi^v_{(i,j,k)_\alpha} - \phi^v_{i,j,k}\right) \tag{21a}$$

and HCR-2

$$\mathcal{F}^v_{i,j,k} = \frac{1}{\Delta x}\left(\tilde{r}^{i,j,k} \sum_{\alpha=1}^{M_{i,j,k}} \phi^v_{(i,j,k)_\alpha} - \phi^v_{i,j,k}\right). \tag{21b}$$

Note, HCR-2 can be implemented more efficiently since only one constant per cell, $\tilde{r}^{i,j,k}$, needs to be stored, while for HCR-1 the constants $r^{i,j,k}_{(i,j,k)_\alpha}$ need to be stored for each cell.

At this point, a remark regarding the above choice of the weighting factor β is warranted. As remarked in [9], the principle of the CR schemes can be summarized as follows. Provided an approximation of the signed distance function d is given on Γ, a correction Δd for the signed distance is applied on one side of the interface to compensate for the displacement of the interface, see Fig. 1(a) and (b). This correction is translated above into a forcing term ψ to obtain Eqs. (16) and (20). If this forcing is used only on one side of the interface it is reasonable to use $\beta = 1$. However, preliminary numerical experiments not reported in this paper showed for the HCR schemes a distributed forcing on all cells in Γ to yield smoother results than the one-sided forcing. Referring to the CR schemes in the one-dimensional case, a distributed correction for the signed distance function with a weighting factor of 0.5 yields the exact correction of the interface displacement, as illustrated by Fig. 1(c). To account for the forcing on both sides of the interface in the HCR schemes, the weighting factor is therefore set $\beta = 0.5$.

Using a forward Euler integration in pseudo time τ, Eq. (15) can be written in a discretized form using Eqs. (17) and (18)

$$\phi^{v+1}_{i,j,k} = \phi^v_{i,j,k} - \Delta\tau\left\{S(\tilde{\phi})\left(\mathcal{G}\left(D^+_\zeta\phi^v_{i,j,k}, D^-_\zeta\phi^v_{i,j,k}\right) - 1\right) - \beta\delta^{\mathcal{F}}_{i,j,k}\mathcal{F}^v_{i,j,k}\right\}, \tag{22a}$$

where Eq. (21) is substituted for $\mathcal{F}^v_{i,j,k}, \zeta = \{x,y,z\}$, the pseudo-time step is $\Delta\tau = \frac{\Delta x}{4}$, and $\mathcal{G}$ is the Godunov Hamiltonian

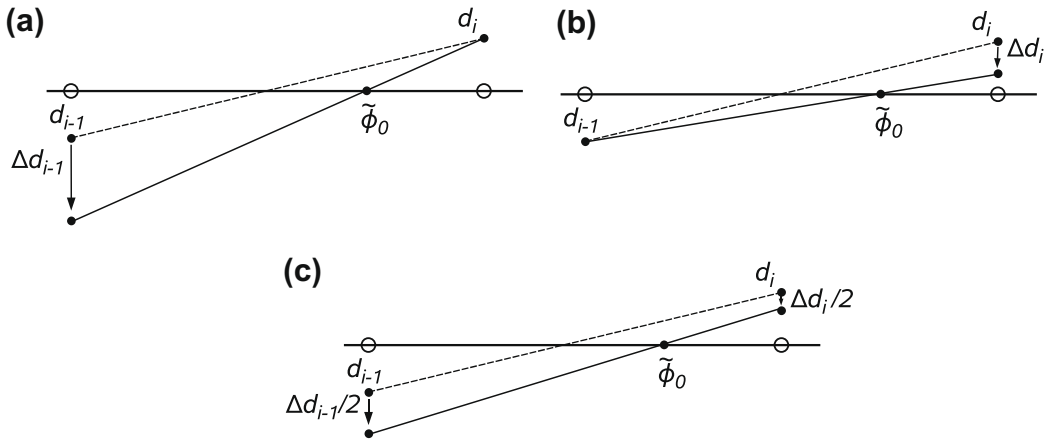

Fig. 1. Illustration of one-sided and two-sided correction of the signed distance function d to compensate for the displacement of the interface: (a) one-sided correction at $\mathbf{x}_{i-1}$ by Δd_{i-1}; (b) one-sided correction at $\mathbf{x}_i$ by Δd_i; (c) two-sided correction at $\mathbf{x}_{i-1}$ by $\Delta d_{i-1}/2$ and at $\mathbf{x}_i$ by $\Delta d_i/2$. The location of the interface before the reinitialization is marked by $\tilde{\phi}_0$ and the open circles show the discrete grid.

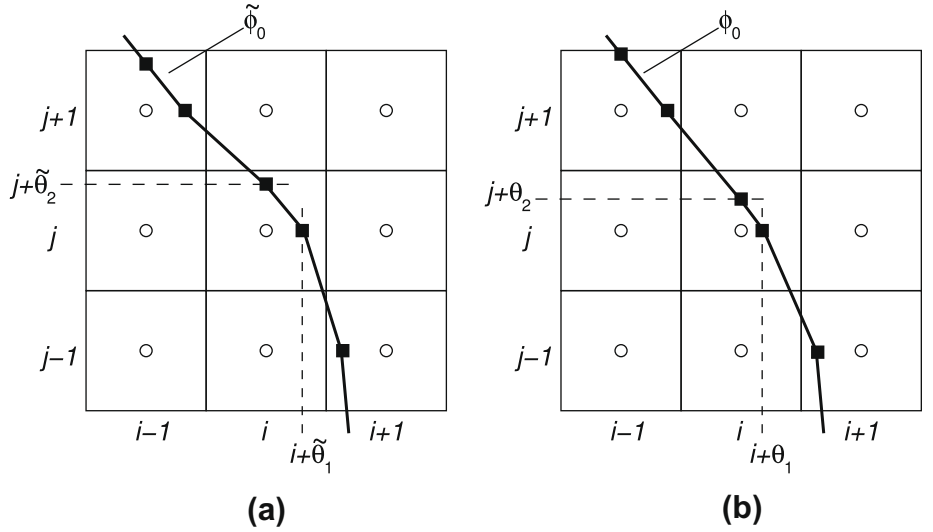

Fig. 2. Illustration of the interface displacement during the reinitialization: (a) sketch of the ϕ_0 contour before the reinitialization; (b) sketch of the ϕ_0 contour after the reinitialization. Circles: grid cell centers, where the level set function is stored; squares: interface locations on ϕ_0 which can be determined by linear interpolation of the level set function ϕ.

$$\mathcal{G}(a,b,c,d,e,f) = \begin{cases} \sqrt{\max(a_+^2, b_-^2) + \max(c_+^2, d_-^2) + \max(e_+^2, f_-^2)} & \text{if } \tilde{\phi}_{i,j,k} \geqslant 0, \\ \sqrt{\max(a_-^2, b_+^2) + \max(c_-^2, d_+^2) + \max(e_-^2, f_+^2)} & \text{if } \tilde{\phi}_{i,j,k} < 0, \end{cases} \tag{22b}$$

with $a_+ = \max(a, 0)$ and $a_- = \min(a, 0)$ and the quantities D_ζ^+ and D_ζ^- denote the discrete forward and backward difference approximation of the derivative with respect to the ζ direction. These operators are computed by the fifth-order Hamilton–Jacobi WENO scheme (WENO-5) of Jiang and Peng [13]. Note, the scheme (22a) is formulated such that for the case of a constant discrete forcing term the amount of forcing per unit pseudo-time is independent of the pseudo-time step $\Delta\tau$.

Finally, we note that the scheme (22a) can be recast into a two-step predictor-corrector type scheme

$$\begin{cases} \phi_{i,j,k}^{\nu+1/2} = \phi_{i,j,k}^{\nu} - \Delta\tau\ S(\tilde{\phi})\Big(\mathcal{G}\Big(D_\zeta^+ \phi_{i,j,k}^{\nu}, D_\zeta^- \phi_{i,j,k}^{\nu}\Big) - 1\Big), \\ \phi_{i,j,k}^{\nu+1} = \phi_{i,j,k}^{\nu+1/2} + \Delta\tau\ \beta\ \delta_{i,j,k}^{\mathcal{F}} \mathcal{F}_{i,j,k}^{\nu+1/2}, \end{cases} \tag{23}$$

where the forcing term acts on the pseudo-time level $v+\frac{1}{2}$ instead of v. We tested both formulations (22a) and (23) and found that the differences in the results are rather small when $\mathcal{O}(10)$ or more iterations are used in the reinitialization steps. The 2-step scheme (23) tends to become superior to the formulation (22a) with a decreasing number of pseudo-time steps. Since, however, the formulation (22a) appears slightly simpler to implement all reported results are obtained with this formulation.

Note that the formulation (23) is conceptually similar to the modified reinitialization scheme proposed in [4] in that a correction of the original reinitialization equation is performed. However, in [4] the correction is applied by enforcing the partial cell volumes on one side of the zero level set to be preserved which, however, could lead to oscillatory solutions as shown in [15]. Unlike this integral correction, the HCR schemes correct the reinitialization by explicitly using certain points on the interface to prevent its displacement.

4.3. Summary of the HCR schemes

To clarify the implementation of the HCR schemes a recap of the formulations HCR-1 and HCR-2 is given. To use the HCR formulations the following steps are to be conducted:

(1) Update the set Γ defined in Eq. (13) such that it contains all cells at the ϕ_0 level set.
(2) Update the set $\mathcal{S}_{i,j,k}$ defined in Eq. (10) for each cell in Γ and let $M_{i,j,k}$ be the number of cells in $\mathcal{S}_{i,j,k}$.
(3a) For the HCR-1 scheme: Compute the constants $r^{i,j,k}_{(i,j,k)_\alpha}$ (Eq. (19a)) for each cell in Γ.
(3b) For the HCR-2 scheme: Compute the constant $\tilde{r}^{i,j,k}$ (Eq. (19b)) for each cell in Γ.
(4) Solve the constrained reinitialization equation by performing the following steps for each iteration:
  (i) Update the set $\mathcal{C}^v$ given by Eq. (18).
  (iia) For the HCR-1 scheme: Compute the forcing terms given by Eq. (21a).
  (iib) For the HCR-2 scheme: Compute the forcing terms given by Eq. (21b).
  (iii) Integrate Eq. (22a).

The forcing terms computed in step (4) drive the level set function on the cells at the ϕ_0 interface to the target values given by Eq. (16a) for HCR-1 and Eq. (16b) for HCR-2. These target values depend on the level set function across the interface and are computed in a similar fashion as the signed distance in the constrained reinitialization schemes CR-1 and CR-2 [9]. Hence, they represent an approximation to the signed distance function on the cells at the front, which is computed such that the difference of the values for θ (Eq. (8d)) and $\tilde{\theta}$ (Eq. (8b)), i.e., the local displacement of the interface, is minimized (HCR-1) or vanishes at certain points on the interface (HCR-2). While in the original constrained reinitialization scheme [9], the signed distance is directly assigned to the level set function as a boundary condition for the iterative solution of the reinitialization equation, the novel HCR schemes blend the evolution of the level set function according to the original reinitialization equation and the assignment of target values to avoid the unwanted displacement of the interface. The resulting constrained reinitialization Eq. (15) can then be discretized in space by higher-order schemes. For details on the derivation of the expressions for the target values the reader is referred to [9].

5. Numerical experiments

To demonstrate the accuracy and robustness of the novel HCR schemes, results of several two-and three-dimensional test cases are reported. In the simulations, the level set equation (3) is discretized in time using a 3-stage third-order accurate TVD Runge–Kutta scheme. For the spatial discretization a fifth-order upwind-central scheme is used [15,9]. Unless otherwise stated, a localized narrow-band level set method is used. For further details, we refer to [9].

5.1. Oscillating circle

First, we discuss the results of the oscillating circle test case [9] to evidence the increased accuracy of the HCR WENO-5 reinitialization in comparison with the lower order CR reinitialization and especially with the standard WENO-5 reinitialization. The extension velocity $\mathbf{f}$, which is extended into the domain using a first-order discretization of the hyperbolic PDE proposed in [10], is specified as $\mathbf{f} = s\mathbf{n}$, where

$$s = \cos(8\Theta)\sin(\omega) \tag{24a}$$

and

$$\Theta = \arctan\left|\frac{y}{x}\right|, \quad \omega = \frac{2\pi t}{t_e}. \tag{24b}$$

The normal vector $\mathbf{n}$ is approximated using a second-order centered difference scheme. An initially circular interface with radius $r = 3$ centered at $(x, y) = (0, 0)$ in a computational domain $\Omega : [-5, 5] \times [-5, 5]$ is considered. It is extended outwards

and inwards until $t = t_e/2$ and then shrunk back into its original shape, which is attained at $t = t_e$ corresponding to $\omega = 2\pi$. The time step is $\Delta t = \frac{\Delta x}{4}$ corresponding to a CFL number of 0.25 and $t_e = 5$ is used. Since in this test case the interface motion is a function of the level set normal vector $\mathbf{n}$ perturbations of the level set function ϕ translate into errors in the extension velocity vector $\mathbf{f}$, which is why the reinitialization is particularly important.

Solutions are computed using the standard reinitialization Eq. (6) and the constrained reinitialization Eq. (15) using both formulations HCR-1 (Eq. (21a)) and HCR-2 (Eq. (21b)). The reinitialization is performed after each time step and a fixed number of 200 iterations is performed to solve the respective reinitialization equations. This allows the investigation of the full impact of the reinitialization on the quality of the solution.

The results obtained on a 256^2-cell grid after one, two, and three consecutive expansions and contractions of the circular interface corresponding to $\omega = 2\pi$, $\omega = 4\pi$, and $\omega = 6\pi$ are summarized in Table 1 in terms of the mean shape error e_s computed for a general three-dimensional problem by

$$e_s = \frac{1}{Nr}\sum_{n=1}^{N}\left(\sqrt{x_n^2 + y_n^2 + z_n^2} - r\right), \tag{25}$$

where N is the number of sample points on the interface $\phi_0$determined by linear interpolation between neighboring cells. For the present two-dimensional test case $z_n = 0$. Both HCR-1 and HCR-2 are able to reduce the mean shape error by an order of magnitude compared to the original reinitialization equation discretized by the fifth-order WENO scheme. Note that the mean shape error e_s contains an error inherent in the linear interpolation by which x_n and y_n are computed. That is, $e_s \neq 0$ for the initial solution at $\omega = 0$. However, the mean shape error which is computed for the initial solution at $\omega = 0$ is about two orders of magnitude smaller than that computed for the solution at $\omega = 2\pi$ after one expansion and contraction of the interface and hence has a negligible influence on the data presented in Table 1. This can also be shown by exactly comparing the solutions at $\omega = 0$ against the solutions at $\omega = 2\pi, \omega = 4\pi$, and $\omega = 6\pi$ using the actual values of the level set function on the cells in Γ, which isolates the solution error. In Table 2, the mean error in the level set function computed for a general three-dimensional problem by

$$e_\Gamma = \frac{1}{\mathcal{N}_\Gamma r}\sum_{\mathbf{x}_{i,j,k}\in\Gamma}\left|\phi_{i,j,k} - \phi_{i,j,k}(\omega = 0)\right|, \tag{26}$$

is summarized showing only slight differences to the results presented in Table 1. In Eq. (26), $\mathcal{N}_\Gamma$ denotes the number of cells in Γ. The results in Tables 1 and 2 are corroborated by the illustrations in Fig. 3, which clearly show the HCR-1 and the HCR-2 solutions at $\omega = 2\pi$ after one expansion and contraction of the interface to be more accurate than the WENO-5 solution, which exhibits artifacts of the oscillatory motion. Fig. 3(a)–(c) show the solutions for the fully expanded interface at $\omega = \pi$ before the contraction to be visually indistinguishable suggesting that the major part of the error in the WENO-5 solutions is caused during the contraction of the expanded interface. For the fully expanded interface at $\omega = \pi$, contours of the level set function are plotted in Fig. 4. The solution from a full-domain standard level set method without reinitialization shown in Fig. 4(a) is contrasted with narrow-band level set solutions obtained using the HCR-1 and HCR-2 schemes shown in Fig. 4(b) and (c), respectively. The comparison illustrates the effect of the reinitialization procedure, which regularizes the strained level set field evidenced in Fig. 4(a).

Table 1
Mean shape error e_s at different time levels for the oscillating circle test case. Comparison of the solutions computed by the original reinitialization equation (6) and the novel constrained reinitialization equation (15) on a 256^2-cell grid. The WENO-5 scheme is used for the spatial discretization of the respective reinitialization equations.

Reinitialization scheme	$\omega = 2\pi$	$\omega = 4\pi$	$\omega = 6\pi$
Original WENO-5	1.762×10^{-2}	3.285×10^{-2}	4.557×10^{-2}
HCR-1 WENO-5	1.444×10^{-3}	2.919×10^{-3}	4.406×10^{-3}
HCR-2 WENO-5	1.265×10^{-3}	2.554×10^{-3}	3.854×10^{-3}

Table 2
Mean error e_Γ of the level set function at different time levels for the oscillating circle test case. Comparison of the solutions computed by the original reinitialization equation (6) and the novel constrained reinitialization equation (15) on a 256^2-cell grid. The WENO-5 scheme is used for the spatial discretization of the respective reinitialization equations.

Reinitialization scheme	$\omega = 2\pi$	$\omega = 4\pi$	$\omega = 6\pi$
Original WENO-5	1.626×10^{-2}	3.046×10^{-2}	4.271×10^{-2}
HCR-1 WENO-5	1.452×10^{-3}	2.942×10^{-3}	4.440×10^{-3}
HCR-2 WENO-5	1.275×10^{-3}	2.579×10^{-3}	3.890×10^{-3}

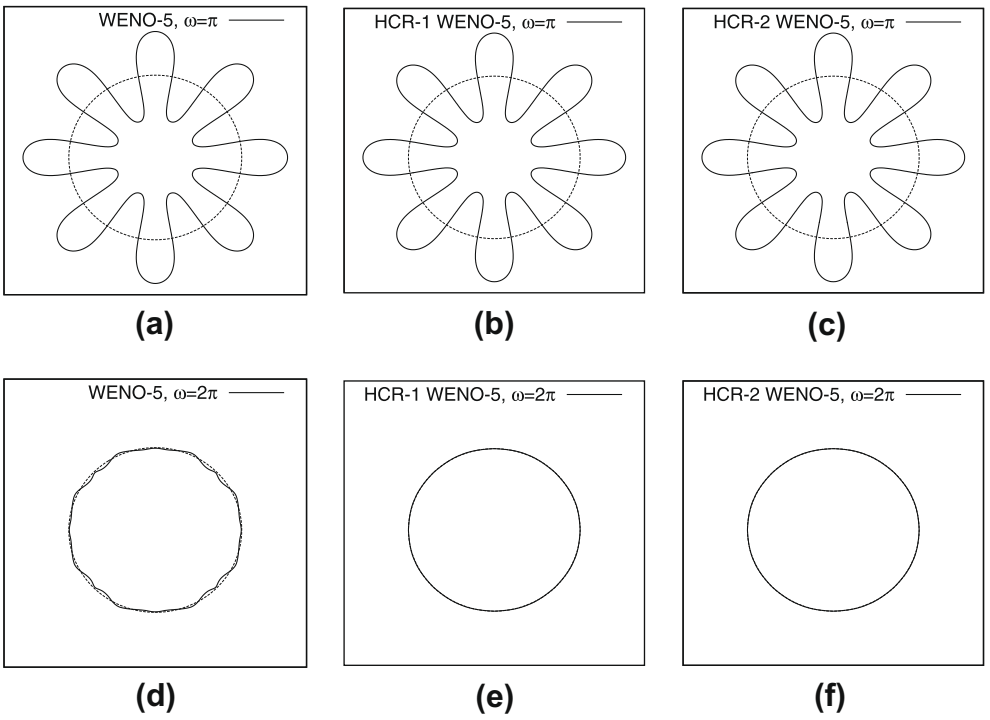

Fig. 3. Oscillating circle test case. Comparison of the solutions after a full expansion of the interface at $\omega = \pi$ (a–c) and after a full expansion and retraction of the interface at $\omega = 2\pi$ (d–f) obtained on a 256^2-cell grid using different reinitialization schemes: (a and d) original reinitialization equation (6) discretized by WENO-5; (b and e) HCR-1 (Eqs. (15) and (21a)); (c and f) HCR-2 (Eqs. (15) and (21b)). Dashed lines: initial zero level set.

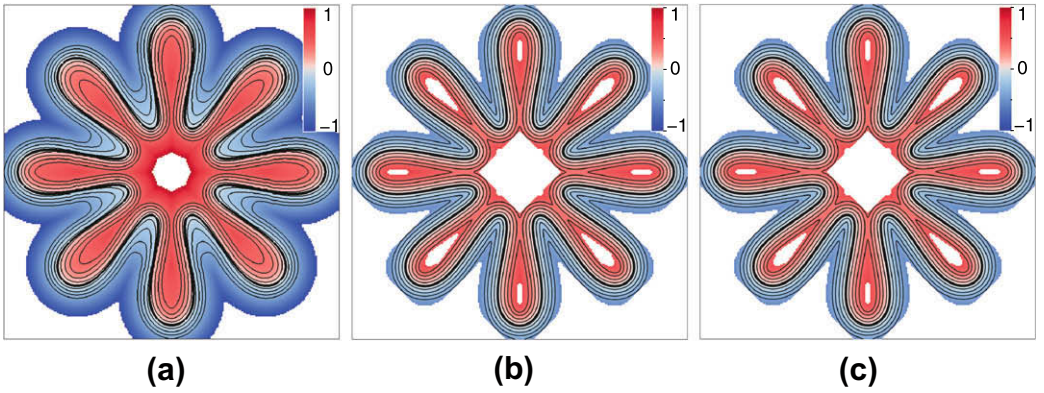

Fig. 4. Oscillating circle test case. Comparison of the scalar level set field after a full expansion of the interface at $\omega = \pi$: (a) full-domain standard level set method without reinitialization; (b) localized level set method using HCR-1 (Eqs. (15) and (21a)); and (c) localized level set method using HCR-2 (Eqs. (15) and (21b)). Contours of the level set function are evenly spaced by $\Delta\phi = 0.1$ in the range $\phi = \{-0.4, \ldots, 0.4\}$; the ϕ_0 contour is emphasized as a thick line. The colors correspond to the value of the level set function ϕ; only those cells where $-1 \leqslant \phi \leqslant 1$ are shown. In (b) and (c), the depicted cells correspond to the narrow computing band.

Table 3
Mean shape error e_s at $\omega = 2\pi$ after one expansion and contraction of the interface for solutions of the oscillating circle test case obtained on different grids. Comparison of the solutions computed by the original reinitialization equation (6) and the novel constrained reinitialization equation (15). The WENO-5 scheme is used for the spatial discretization of the respective reinitialization equations.

Reinitialization scheme	Grid			
	64^2	128^2	256^2	512^2
Original WENO-5	9.553×10^{-2}	3.467×10^{-2}	1.762×10^{-2}	7.990×10^{-3}
HCR-1 WENO-5	8.031×10^{-3}	2.961×10^{-3}	1.444×10^{-3}	7.128×10^{-4}
HCR-2 WENO-5	7.400×10^{-3}	2.587×10^{-3}	1.265×10^{-3}	6.268×10^{-4}

To analyze the convergence behavior of the various reinitialization schemes solutions have been computed using different grid resolutions. The data is summarized in terms of the mean shape error e_s in Table 3 showing first-order convergence for all investigated reinitialization schemes. More importantly, the results evidence the accuracy improvement regarding the mean shape error to be approximately one order of magnitude for the HCR-1 and HCR-2 schemes on all grids.

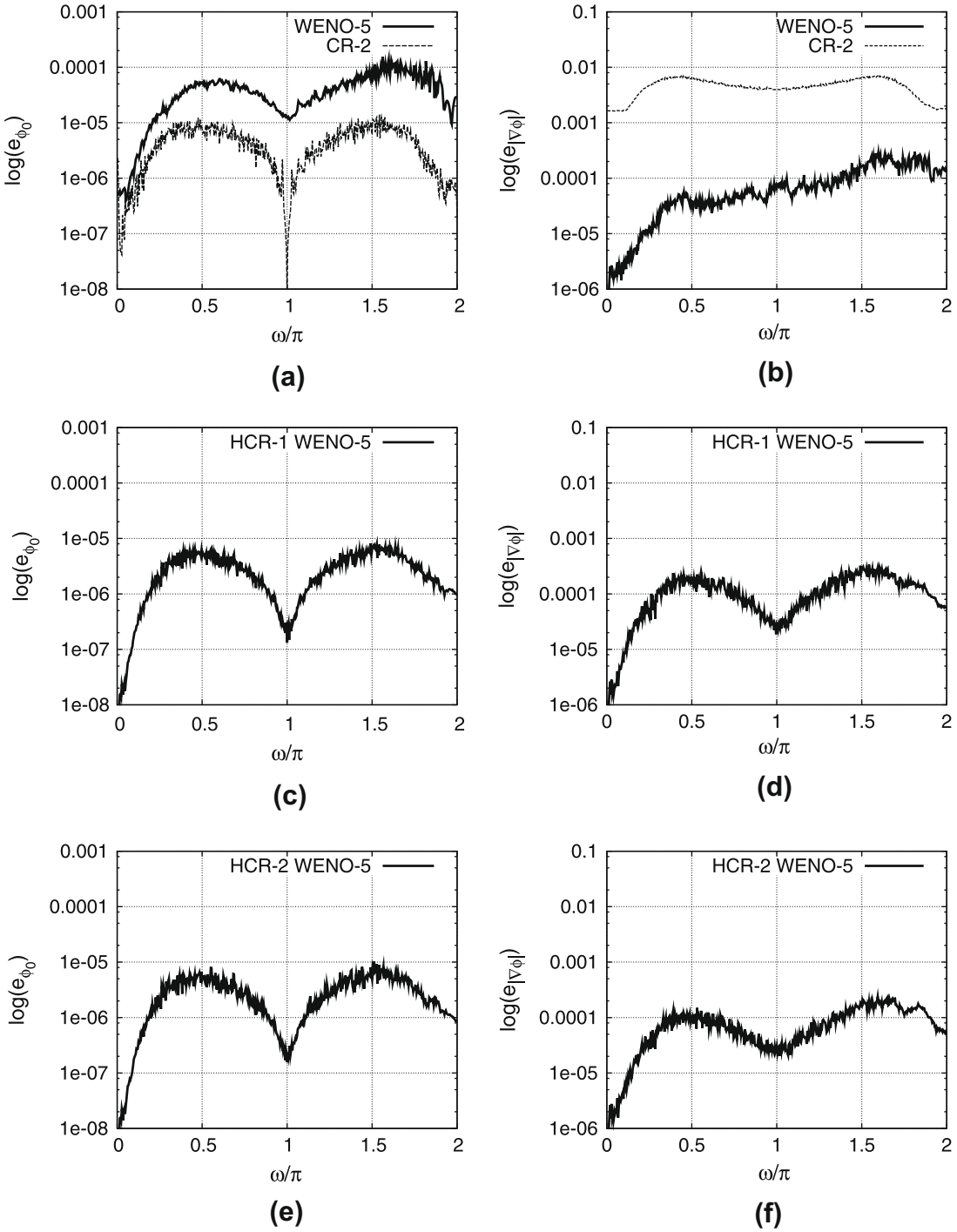

Fig. 5. Oscillating circle test case. Comparison of solutions obtained on a 256^2-cell grid using different reinitialization schemes: (a, c, e) mean displacement e_{ϕ_0} (Eq. (27)) of the zero level set ϕ_0 due to the reinitialization; (b, d, f) mean deviation $e_{|\nabla\phi|}$ computed by Eq. (28) on the cells in Γ after the reinitialization steps.

In Fig. 5 more detailed data on the performance of the different reinitialization schemes is presented for the solutions obtained on a 256^2-cell grid. The mean displacement of the interface is computed by

$$e_{\phi_0} = \frac{\Delta x}{N} \sum_{n=1}^{N} |\theta_n - \tilde{\theta}_n|, \tag{27}$$

where again N is the number of sample points on the interface ϕ_0 determined by linear interpolation between neighboring cells and θ and $\tilde{\theta}$ are computed as in Eqs. (8d) and (8b), respectively. The mean deviation from the signed distance property $|\nabla\phi| = 1$ is computed after each reinitialization step by

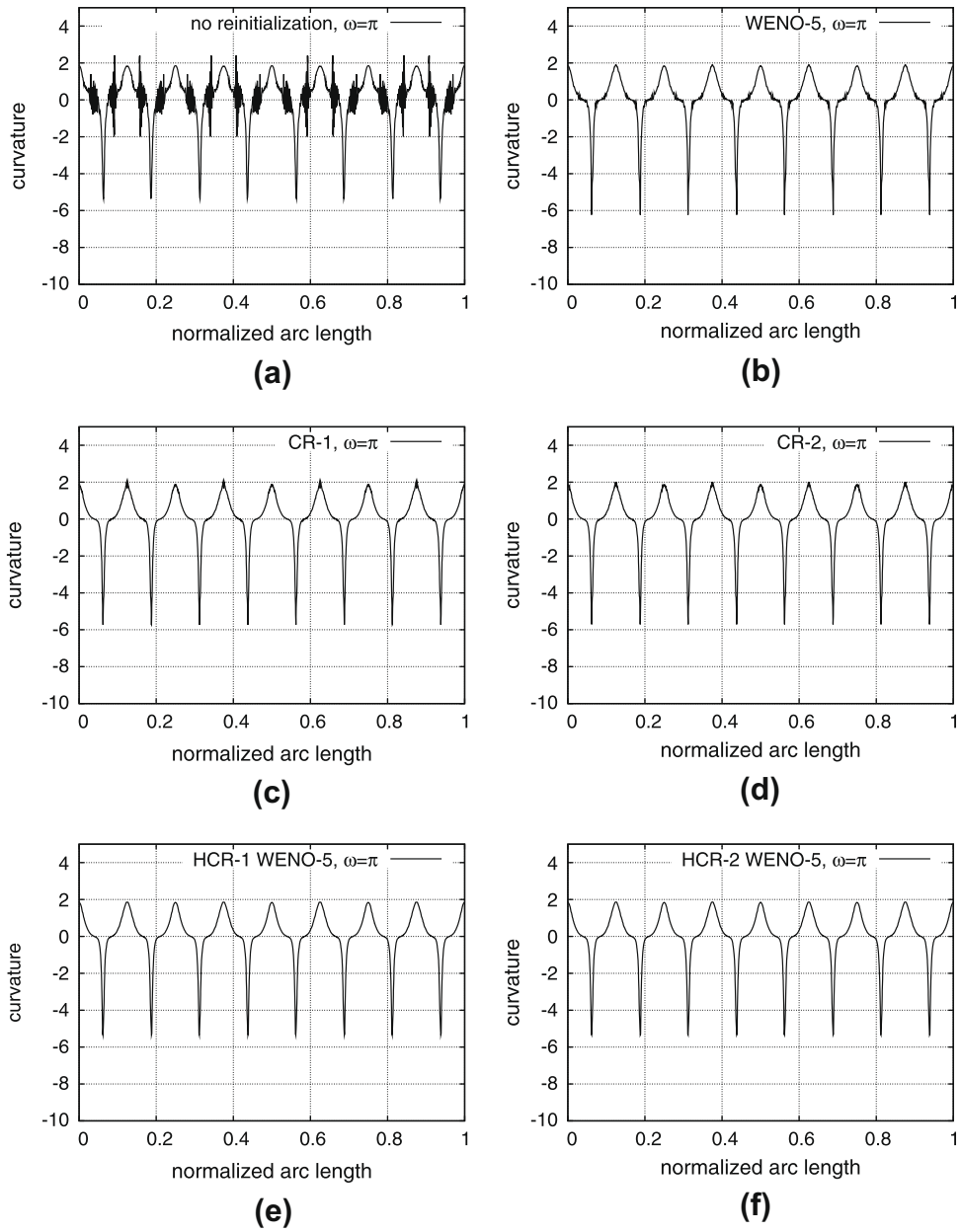

Fig. 6. Oscillating circle test case. Comparison of the ϕ_0 curvature along the zero level set for the solutions at $\omega = \pi$ after one expansion obtained on a 256^2-cell grid using different reinitialization schemes: (a) full-domain standard level set method without reinitialization; (b) original reinitialization equation (6) discretized by WENO-5; (c) CR-1 [9]; (d) CR-2 [9]; (e) HCR-1 (Eqs. (15) and (21a)); and (f) HCR-2 (Eqs. (15) and (21b)).

$$e_{|\nabla\phi|} = \frac{1}{\mathcal{N}_\Gamma} \sum_{\mathbf{x}_{i,j,k} \in \Gamma} ||\mathbf{\nabla}\phi|_{i,j,k} - 1|| \tag{28}$$

in the general three-dimensional form, where a fourth-order central scheme is used to compute the derivatives of the level set function. As a reference, the respective solutions obtained with the constrained reinitialization scheme CR-2 [9,12] are shown in Fig. 5(a) and (b). Fig. 5(a), (c), and (e) clearly show the displacement of the interface caused by the standard WENO-5 reinitialization to be roughly an order of magnitude larger than that of CR-2 and the novel formulations HCR-1 and HCR-2. In terms of this interface displacement, HCR-1 and HCR-2 possess a solution quality like CR-2. The benefit of using a higher-order discretization in HCR-1 and HCR-2 can be observed in Fig. 5(b), (d), and (f), where the mean deviation $e_{|\nabla\phi|}$ is illustrated. The solutions obtained with the fifth-order HCR-1 and HCR-2 reinitialization are significantly more accurate than the lower-order scheme CR-2 and compare favorably with the standard WENO-5 reinitialization scheme. This is an especially important result since it shows that the forcing terms are able to significantly reduce the interface displacement during the reinitialization without compromising the accuracy to which the property $|\mathbf{\nabla}\phi| = 1$ is approximated.

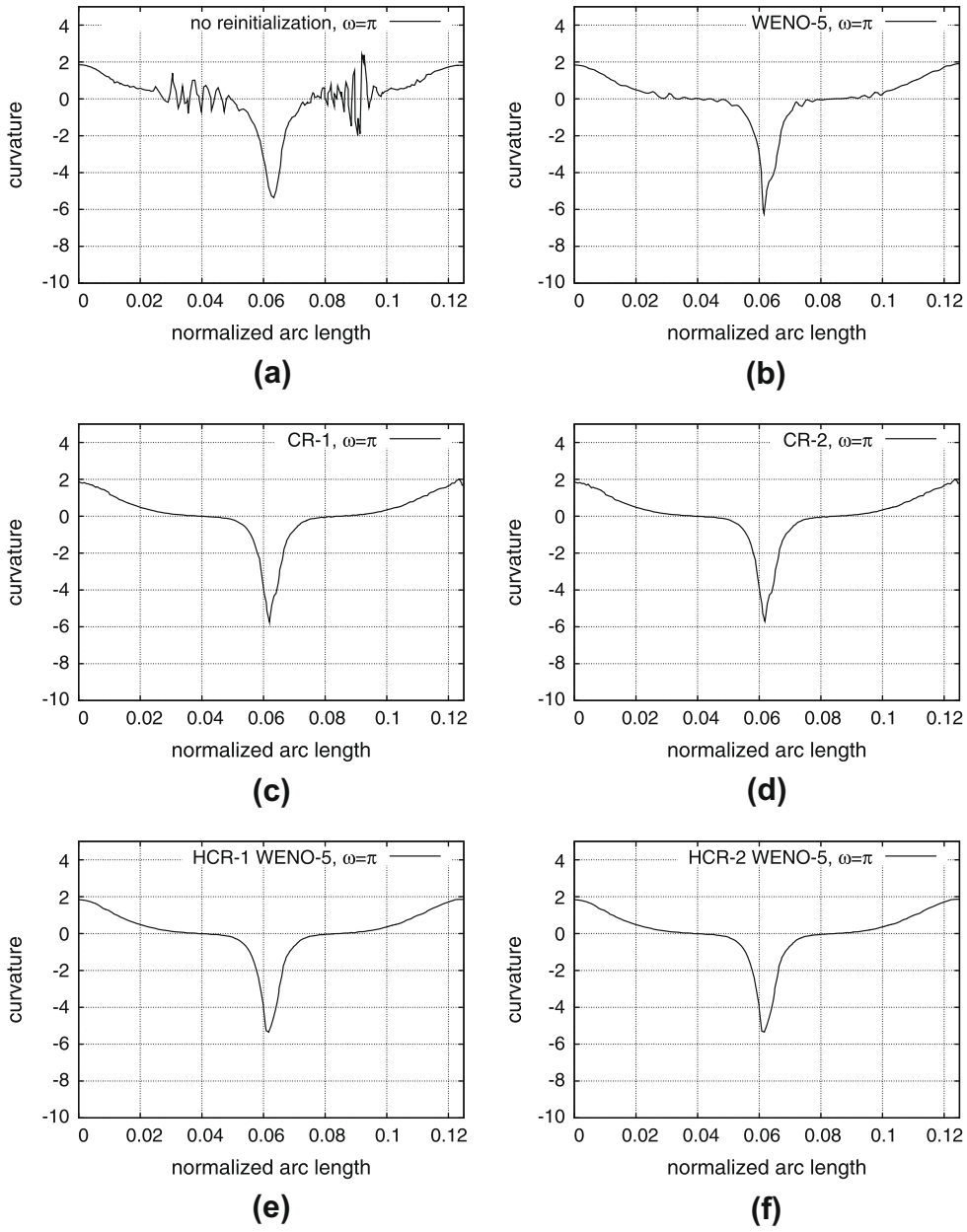

Fig. 7. Close-up view of the results plotted in Fig. 6.

From the accurate approximation of $|\nabla\phi| = 1$ by HCR-1 and HCR-2 one can infer a smooth approximation of higher derivatives of the level set function using these reinitialization schemes. In this context, an important quantity appearing as a model parameter in several level set applications such as multiphase flow and premixed combustion is the curvature $\mathfrak{C}$ defined in Eq. (4b). For the oscillating circle test case, the solutions which are obtained using the different reinitialization schemes closely match at $\omega = \pi$ as indicated in Fig. 3(a)–(c), such that the curvature distribution along the zero level set contour can be compared. In Fig. 6, the curvature is plotted over the normalized arc length of the ϕ_0 contour for the different reinitialization schemes and for a full-domain standard level set computation without reinitialization (Fig. 6(a)). In Fig. 7, a close-up view of the results is presented. The curvature of the ϕ_0 contour is obtained by linear interpolation of the curvature computed on the cells in Γ. Figs. 6 and 7(a) clearly show the computed ϕ_0 curvature to contain spurious waves when no reinitialization is performed, that is, when perturbations in the level set solution are not removed and thus can accumulate and the level set field is strained as illustrated for this case in Fig. 4(a). Using the WENO-5 original reinitialization (6) significantly smoothens the curvature distribution along the ϕ_0 arc, but high-frequency oscillations at a lower amplitude than those appearing in the solutions without a reinitialization remain. This is illustrated in Figs. 6 and 7(b). In terms of a smooth ϕ_0 curvature distribution, a further significant improvement is gained when the constrained reinitialization scheme is used in its original formulations CR-1 and CR-2 [9] in conjunction with a first-order spatial discretization to reconstruct $|\nabla\phi| = 1$. The corresponding results are shown in Figs. 6 and 7(c) for CR-1 and in Figs. 6 and 7(d) for CR-2, respectively. From the fact that the curvature distribution is smoother when CR-1 or CR-2 is used than when the higher-order standard WENO-5 reinitialization is employed the oscillations in the WENO-5 curvature distribution can be traced back to the displacement of the

Table 4
Mean shape error e_s at $\omega = 2\pi$ after one expansion and contraction of the interface for the oscillating circle test case. Comparison of the solutions computed by the original reinitialization equation (6) and the novel constrained reinitialization equation (15) on a 256^2-cell grid at various numbers of iterations for the reinitialization. The WENO-5 scheme is used for the spatial discretization of the respective reinitialization equations.

Reinitialization scheme	Number of iterations		
	20	200	2000
Original WENO-5	1.165×10^{-2}	1.762×10^{-2}	4.113×10^{-2}
HCR-1 WENO-5	1.499×10^{-3}	1.444×10^{-3}	1.447×10^{-3}
HCR-2 WENO-5	1.339×10^{-3}	1.265×10^{-3}	1.266×10^{-3}

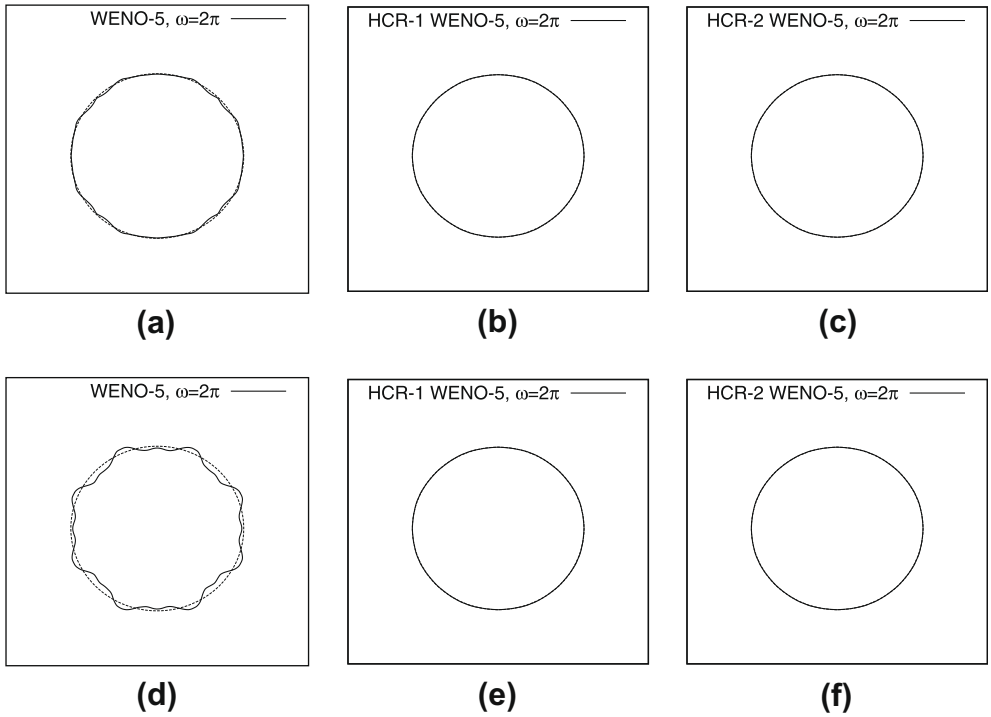

Fig. 8. Oscillating circle test case. Comparison of the solutions after a full expansion and retraction of the interface at $\omega = 2\pi$ obtained on a 256^2-cell grid using 20 pseudo-time steps (a–c) and 2000 pseudo-time steps (d–f) at different reinitialization schemes: (a and d) original reinitialization equation (6) discretized by WENO-5; (b and e) HCR-1 (Eqs. (15) and (21a)); (c and f) HCR-2 (Eqs. (15) and (21b)). Dashed lines: initial zero level set.

interface during the reinitialization, which become manifest in local perturbations of the ϕ_0 contour. Finally, the novel high-order constrained reinitialization schemes HCR-1 and HCR-2 deliver the smoothest curvature distribution showing no visible fluctuations, as illustrated in Figs. 6 and 7(e) and (f).

To demonstrate the robustness of the HCR schemes with regard to the influence of the number of iterations performed for the reinitialization, additional simulations were run with 20 and 2000 pseudo-time steps in each reinitialization step. The results at $\omega = 2\pi$ after a full expansion and retraction of the interface are summarized in Table 4 and illustrated in Fig. 8, the plots of which correspond to Fig. 3(d–f) for the simulation with 200 iterations in each reinitialization step. Furthermore, the interface location error $\Delta x|\theta - \tilde{\theta}|$ along the arc is plotted and juxtaposed in Fig. 9 for the solutions at $\omega = 2\pi$ computed using the different reinitialization schemes and various numbers of performed pseudo-time steps. It is evident that the quality of the WENO-5 results degrades with an increasing number of pseudo-time steps, whereas the HCR-1 and HCR-2 results hardly change or slightly improve. Furthermore, the plots in Fig. 9 show that the interface location error is in the solutions obtained with the standard WENO-5 reinitialization between one and two orders of magnitude larger than with HCR-1 and HCR-2. Hence, with the novel HCR schemes the solution of the Eikonal equation can be converged as far as required without deteriorating the accuracy through interface displacement.

5.2. Vortex deformation of a circle

An established test case for level set methods is the deformation of a circular interface by a single time-dependent vortex [16,2]. In this test case the circular interface is deformed into a spiral shape with a sharp end. Initially, the circle with a radius of 0.15 is centered at $(x, y) = (0.5, 0.75)$ in a computational domain $\Omega : [0, 1] \times [0, 1]$. The interface is deformed by a time-dependent velocity field given by the stream function

$$\Psi(\mathbf{x}, t) = \frac{1}{\pi} \sin^2(\pi x) \cos^2(\pi y) \cos\left(\frac{\pi t}{T}\right), \tag{29}$$

such that the extension velocity can be prescribed independent of the level set field by $\mathbf{f} = (\partial_y \Psi, -\partial_x \Psi)^T$. The maximum deformation is reached at $t = T/2$, after which the interface deformation is reversed to attain the initially circular shape

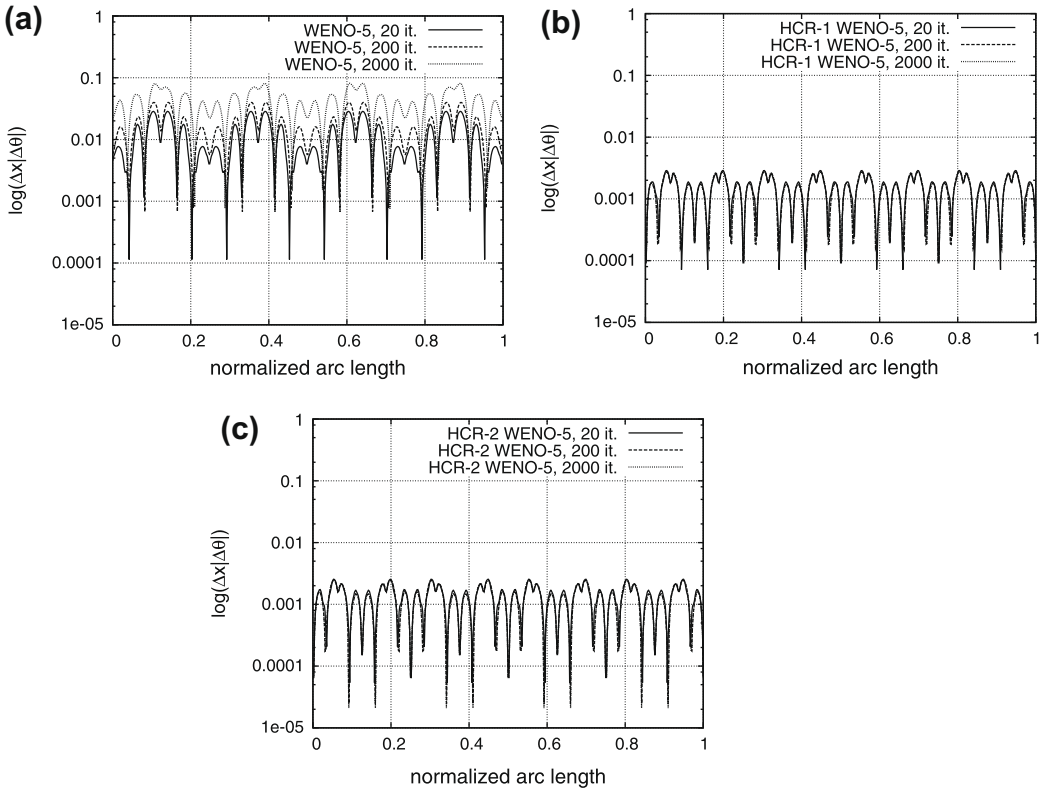

Fig. 9. Oscillating circle test case. Comparison of the interface location error $\Delta x|\theta - \tilde{\theta}|$ over the normalized arc length for the solutions at $\omega = 2\pi$ computed on a 256^2-cell grid using a different number of iterations for the investigated reinitialization schemes: (a) original reinitialization equation (6) discretized by WENO-5; (b) HCR-1 (Eqs. (15) and (21a)); and (c) HCR-2 (Eqs. (15) and (21b)).

at $t = T$, where $T = 8$ is used. For the computations with reinitialization 200 iterations are performed to solve the respective reinitialization equations after each time step. The level set Eq. (3) is solved using a time step of $\Delta t = \Delta x$.

It is demonstrated in [7,15] that a critical factor for an accurate level set solution of the vortex deformation test case is the grid resolution, since the sharp end of the spiral-shaped interface fails to be resolved when its size falls below the mesh size. Furthermore, it is worth noting that the best results at $t = T$ can be obtained for this test case when a reinitialization is not performed and a full-domain standard level set method is used, which is what preliminary computations showed and what is reported in [6]. This is because the interface motion is prescribed and does not depend on derivatives of the level set function as for example in the oscillating circle test case presented in Section 5.1. In the latter test case, a strained or perturbed level set field results in errors of the actual level set extension velocity, which is why the reinitialization is crucial to accurately describe the motion of the ϕ_0 interface. Since in the vortex deformation test case the extension velocity field from $t = 0$ until $t = T/2$ is exactly reversed from $t = T/2$ until $t = T$, so is the straining of the level set field reversed and the associated steep and small gradients of the level set function are removed. In contrast, the changes of the level set field and in particular those of the ϕ_0 contour which are introduced by the reinitialization cannot be exactly reversed, such that the solution accuracy at $t = T$ degrades when the reinitialization is intensively used in this test case.

Nevertheless, the vortex deformation test case allows to investigate the robustness of the novel HCR schemes against the standard reinitialization scheme when the interface forms a thin shape. To this end, a reference solution is computed on a 1024^2-cell grid using a full-domain standard level set method without reinitialization. The development of the interface is illustrated in Fig. 10 showing no visual difference between the solutions during the forward and backward motion. The solutions at $t = T/2$ obtained on different grids and with different reinitialization methods are plotted in Fig. 11. The dashed lines in these plots correspond to the reference solution. It can be observed in Fig. 11(a), (d), and (g) that a significant part of the sharp end of the spiral-shaped interface is lost in the simulations using the standard WENO-5 reinitialization. In contrast, the solutions obtained with the HCR-1 and HCR-2 schemes capture the thin parts of the interface as far as the grid resolution allows and largely match the reference solution. This is remarkable given the fact that the reference solution has been computed on a 1024^2-cell grid.

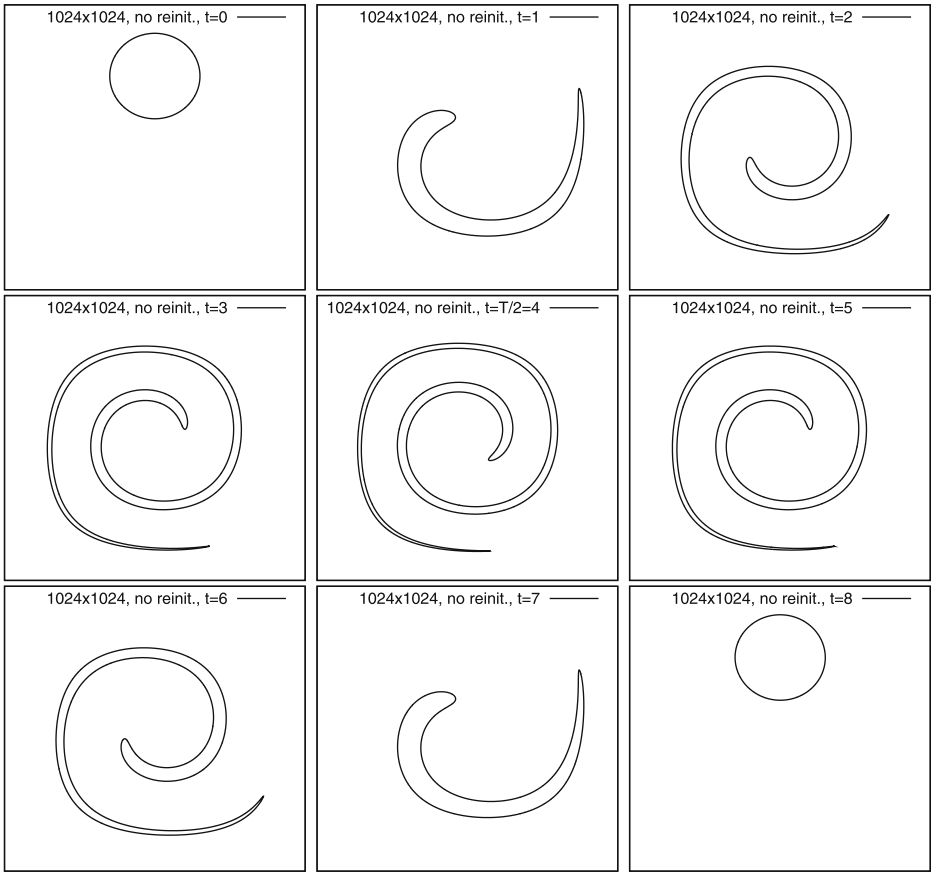

Fig. 10. Vortex deformation test case. Reference solution at different times obtained on a 1024^2-cell grid using a full-domain standard level set method without reinitialization.

It is interesting to compare the results with and without reinitialization on the same grids to understand the effect of the reinitialization on the solution. Such a comparison is presented in Fig. 12, in which contours of the level set field at $t = T/2$ are plotted for full-domain standard level set solutions without reinitialization in Fig. 12(a) and (b) and localized level set solutions with HCR-1 and HCR-2 in Fig. 12(c) and (d) and Fig. 12(e) and (f), respectively. Fig. 12(a), (c), and (e) show the solutions obtained on a 256^2-cell grid and Fig. 12(b), (d), and (f) those on a 512^2-cell grid. Comparing the ϕ_0 contours plotted as thick lines it is evident that the sharp end of the spiral-shaped interface is shorter in the solutions without reinitialization than in those with HCR-1 and HCR-2 reinitialization and that in terms of the elongation of the spiral the HCR-1 and HCR-2 solutions agree closer with the reference solution shown in Figs. 10 and 11. However, it can also be observed that the sharp spiral end is thickened when the reinitialization is used. A comparison of Fig. 12(c) and (d) for the HCR-1 solutions and of Fig. 12(e) and (f) for the HCR-2 solutions shows the thickening to be more significant on the coarser grid than on the finer grid.

Furthermore, the contour lines in Fig. 12(a) and (b) show that the level set function is strained along the spiral axis and compressed in the normal direction to the interface when no reinitialization is used. The comparison of the solutions on two different grids in Fig. 12(a) and (b) evidences that the straining and compression is caused by the prescribed extension velocity and is not a grid effect. As Fig. 12(c–f) indicate, this straining and compression can be completely removed using the reinitialization, while the level set function remains smooth also near the sharp end of

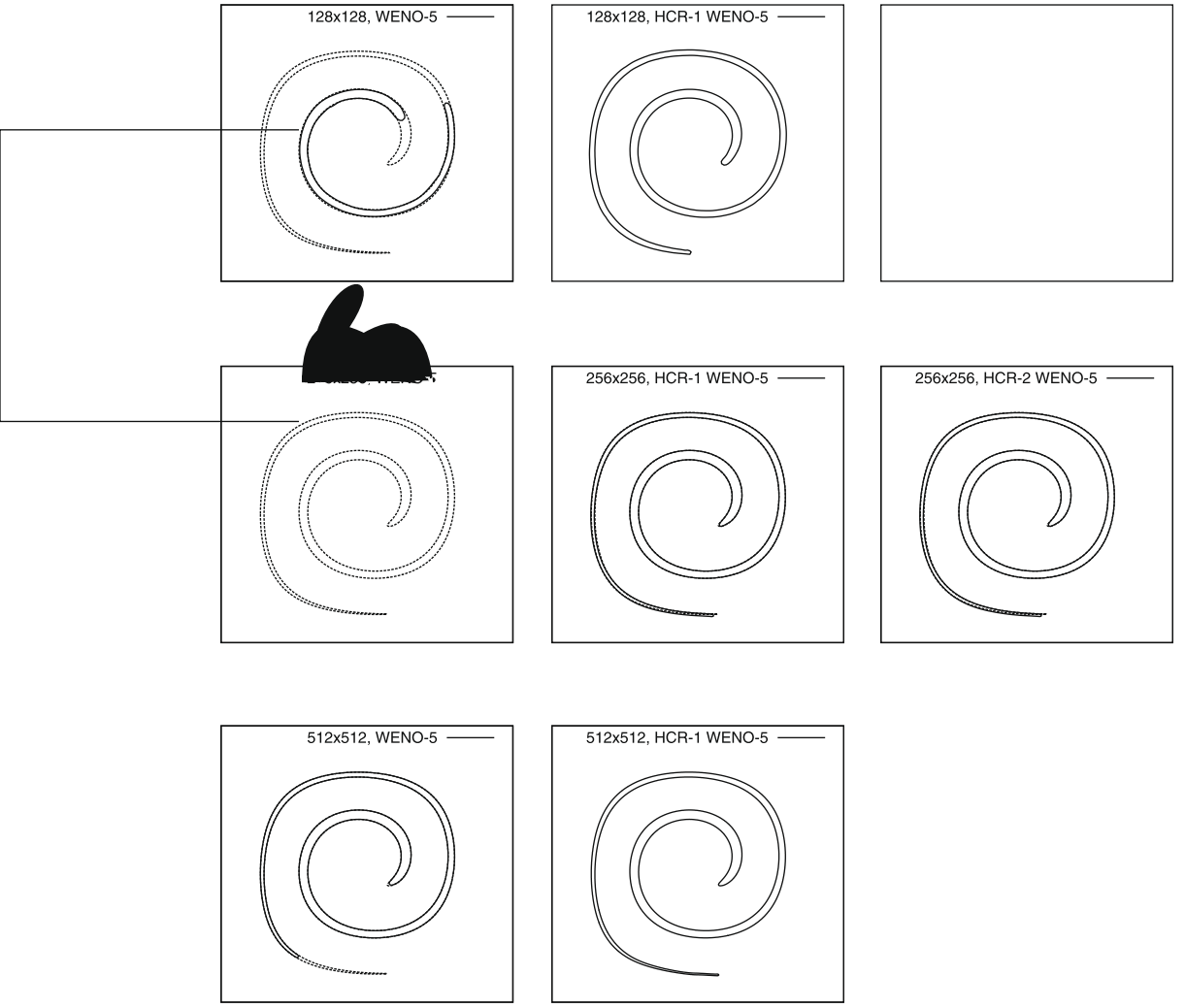

the spiral-shaped interface. However, as aforementioned unlike in the oscillating circle test case presented in Section 5.1 removing these irregularities does not appear to be significantly important concerning the solution at $t = T$ in the vortex deformation test case.

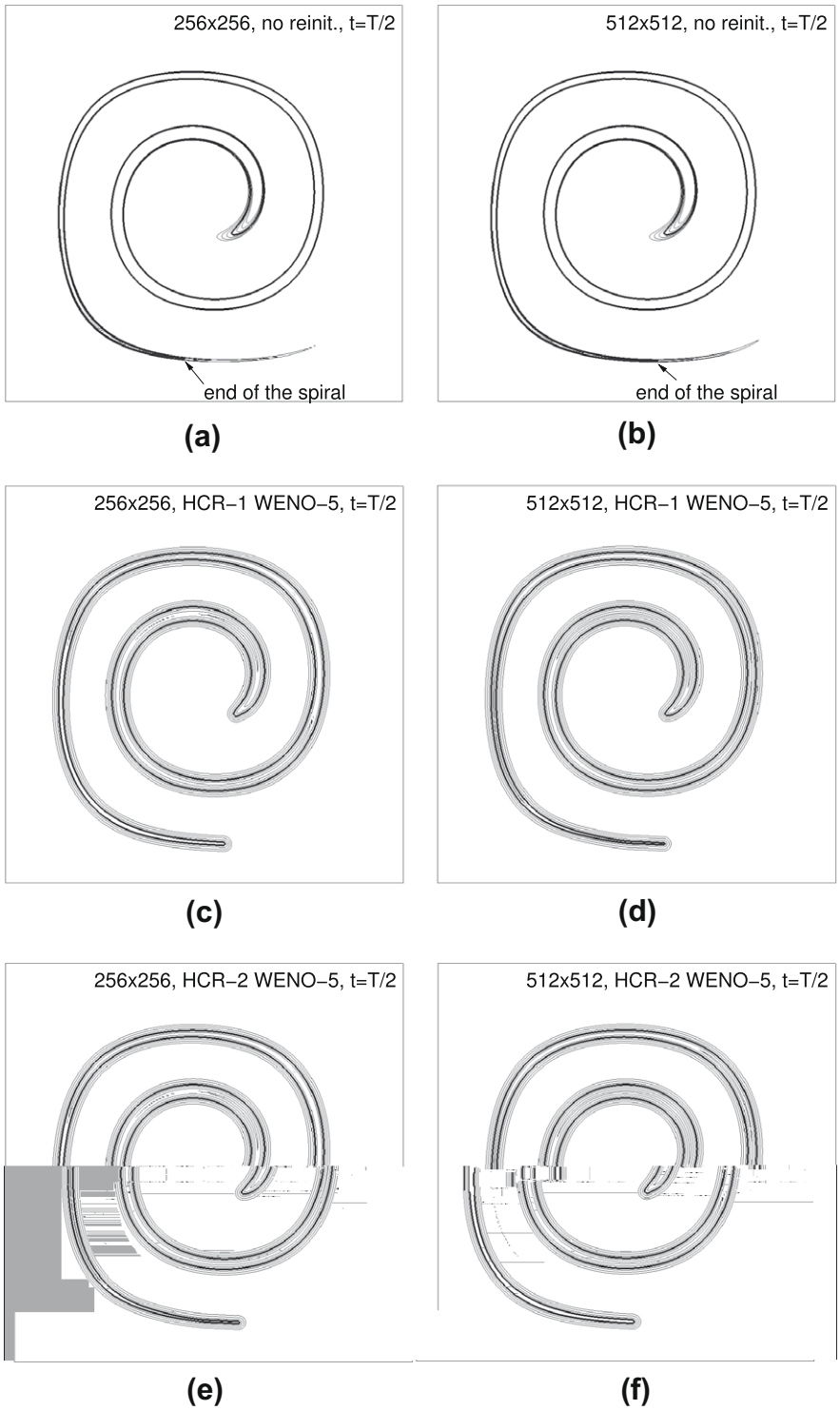

Fig. 12. Vortex deformation test case. Effect of the reinitialization on different grids at $t = T/2$: (a, c, e) 256^2-cell grid; (b, d, f) 512^2-cell grid. (a and b) Comparison of solutions obtained with a full-domain standard level set method without reinitialization, a localized level set method using (c and d) HCR-1 and (e and f) HCR-2. Contour lines are plotted in intervals of $\Delta\phi = 0.005$ in the range from $\phi = -0.015$ to $\phi = 0.015$. The ϕ_0 contour is plotted as a thick line.

5.3. Three-dimensional coalescing interfaces

To demonstrate the smoothness of the novel HCR schemes results of a three-dimensional test case, in which the interface topology changes, are concisely presented. In this test case three spherical interfaces centered at $(x,y,z)_1 = (1.0, 1.5, 1.5)$, $(x,y,z)_2 = (-1.7, 1.5, 1.5)$, and $(x,y,z)_3 = (-0.5, -0.5, -0.5)$ at radii $r_1 = 1.2, r_2 = 1.0$, and $r_3 = 0.8$ are expanded at the constant speed $s = 1$. The computational domain $\Omega : [-5,5] \times [-5,5] \times [-5,5]$ is discretized by 128^3 cells. Otherwise, the same set up as for the previous test case is used with a CFL number of $\approx$0.25. The temporal development of the WENO-5, the HCR-1, and the HCR-2 solutions using 200 iterations for each reinitialization step is qualitatively shown in Fig. 13 for three time levels. The illustration evidences for all schemes the smooth coalescence of two (Fig. 13(d)–(f)) and finally three spherical

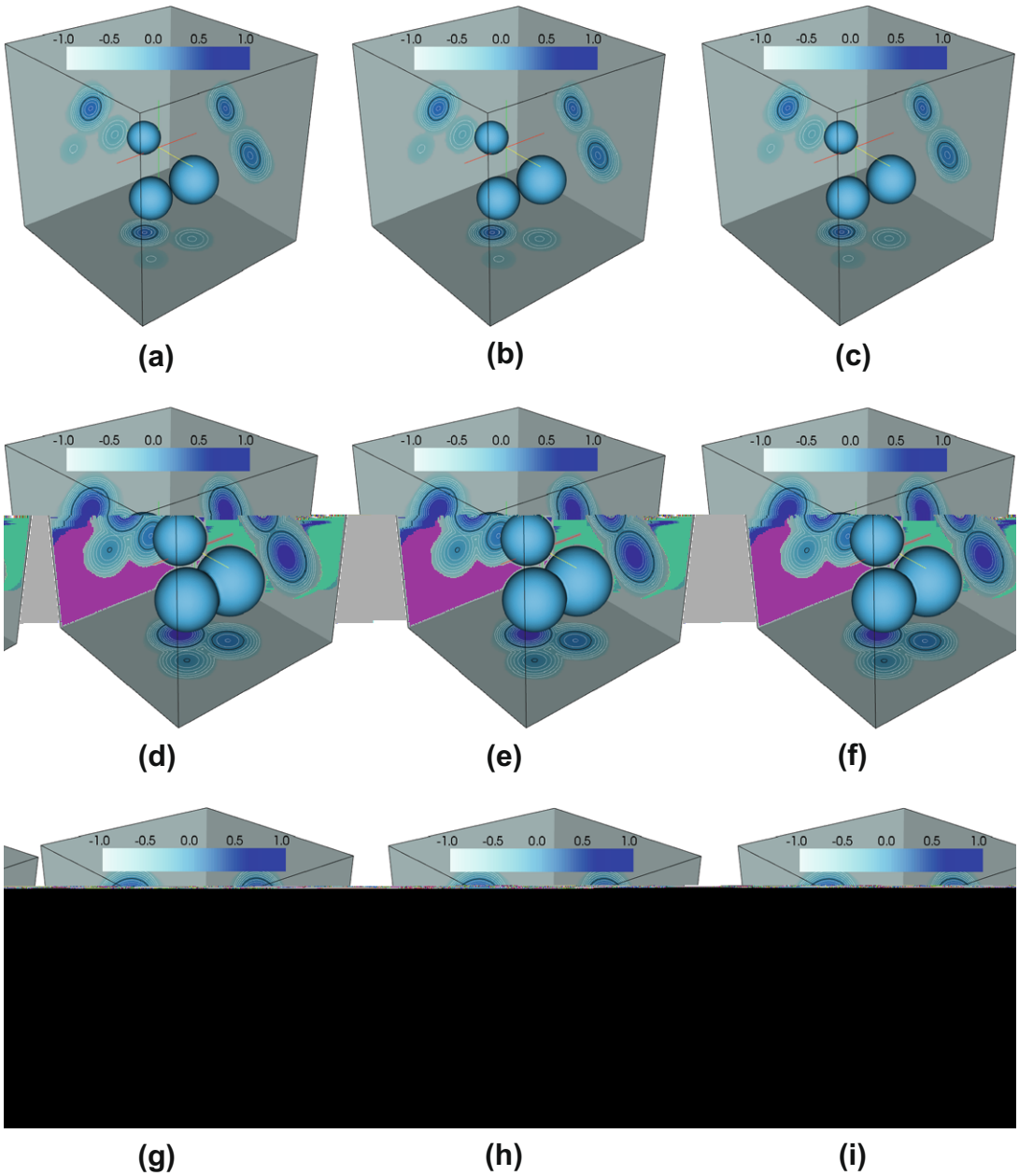

Fig. 13. Coalescing spherical interfaces. Comparison of solutions obtained on a 128^3-cell grid using different reinitialization schemes: (a, d, g) original reinitialization equation (6) discretized by WENO-5; (b, e, h) HCR-1 (Eqs. (15) and (21a)); (c, f, i) HCR-2 (Eqs. (15) and (21b)). Solutions are shown at different time levels: (a–c) $t = 0$; (d–f) $t = 0.5$; (g–i) $t = 1$. The cut planes show contours of the level set function in the center of the domain. These contours are projected onto the domain boundaries for better visibility. The contours are plotted in intervals of $\Delta\phi = 0.1$. Black lines: ϕ_0 level set.

interfaces (Fig. 13(g–i)). Furthermore, comparing Fig. 13(g–i) reveals the solutions obtained with the HCR schemes to be somewhat sharper than the solutions obtained with the standard WENO-5 reinitialization near the interface intersections.

In Table 5, the mean shape error e_s defined by Eq. (25) at $r = 1$ is summarized for different time levels of the solutions obtained on the 128^2-cell grid and a finer 256^2-cell grid. The corresponding data for the mean error e_Γ, which is computed using Eq. (26) at $r = 1$, is given in Table 6. Despite the uniform motion of the interfaces and the resulting low perturbation of the level set field the differences between the solutions obtained with the standard WENO-5 reinitialization and the HCR-1 and HCR-2 schemes are significant and increasing with time. Similar as in the test case presented in Section 5.2 the standard WENO-5 reinitialization smoothes out the interface regions of large curvature, which emerge where the spherical interfaces coalesce. At $t = 1$, the errors on the fine grid are in the standard WENO-5 solutions roughly one order of magnitude larger than those in the HCR-1 and HCR-2 solutions. Furthermore, compared against the 128^2-cell grid solutions the errors on the fine 256^2-cell grid are reduced by a factor of 2 when the standard WENO-5 reinitialization is used versus a factor of 4 for the novel HCR-1 and HCR-2 schemes. In the limits of the investigated grids, this suggests first-order convergence for the solutions obtained by the standard WENO-5 reinitialization and second-order convergence for the solutions obtained by HCR-1 and HCR-2.

As an integral measure of the solution quality the relative error in the interface surface area e_A is listed in Table 7 for the different solutions. It is computed by

$$e_A = \frac{\sum_{\mathbf{x}_{i,j,k}\in\Gamma}\left\{\int_{V_{i,j,k}}\delta(\phi_{i,j,k})dV - \int_{V_{i,j,k}}\delta(D_{i,j,k})dV\right\}}{\sum_{\mathbf{x}_{i,j,k}\in\Gamma}\int_{V_{i,j,k}}\delta(D_{i,j,k})dV}, \tag{30}$$

where D is the analytical signed distance function at the considered time level, $V_{i,j,k}$ is the cell volume of the cell at $\mathbf{x}_{i,j,k}$, and the delta function is discretely evaluated following [17]. As a general trend, it can be observed that in the solutions obtained by the standard WENO-5 reinitialization surface area is lost, while surface area is gained in the solutions obtained by the HCR-1 and HCR-2 schemes. As could be inferred from the results shown in Tables 5 and 6, the absolute value of the error is largest for the standard WENO-5 reinitialization.

5.4. Computation of signed distance functions

Finally, we concisely demonstrate that the proposed novel HCR schemes are capable of not only correcting a level set function which is close to a signed distance function but also generating a signed distance function from a flat level set profile. Two cases are considered on a 256^2-cell grid in a computational domain $\Omega : [-5, 5] \times [-5, 5]$: (1) a square interface with a side length of 6; (2) a slotted disk [18] with a radius of 3, a slot width of 1 and a slot length of 5. First, the exact signed distance function is computed and the cells on Ω^-, Ω^+, and ϕ_0 are identified. Then, the level set function is initialized as

Table 5
Mean shape error e_s at different time levels for the three-dimensional coalescing interfaces. Comparison of the solutions computed by the original reinitialization equation (6) and the novel constrained reinitialization equation (15) on different grids. The WENO-5 scheme is used for the spatial discretization of the respective reinitialization equations.

Reinitialization scheme	Grid	$t = 0.25$	$t = 0.5$	$t = 1$
Original WENO-5	128^2	3.573×10^{-4}	7.617×10^{-4}	9.483×10^{-4}
	256^2	2.100×10^{-4}	4.174×10^{-4}	6.266×10^{-4}
HCR-1 WENO-5	128^2	3.695×10^{-4}	3.484×10^{-4}	3.070×10^{-4}
	256^2	8.845×10^{-5}	8.927×10^{-5}	8.370×10^{-5}
HCR-2 WENO-5	128^2	3.680×10^{-4}	3.290×10^{-4}	2.904×10^{-4}
	256^2	8.861×10^{-5}	8.683×10^{-5}	7.745×10^{-5}

Table 6
Mean error e_Γ of the level set function at different time levels for the three-dimensional coalescing interfaces. Comparison of the solutions computed by the original reinitialization equation (6) and the novel constrained reinitialization equation (15) on different grids. The WENO-5 scheme is used for the spatial discretization of the respective reinitialization equations.

Reinitialization scheme	Grid	$t = 0.25$	$t = 0.5$	$t = 1$
Original WENO-5	128^2	3.472×10^{-4}	7.387×10^{-4}	9.774×10^{-4}
	256^2	1.730×10^{-4}	3.943×10^{-4}	5.721×10^{-4}
HCR-1 WENO-5	128^2	1.925×10^{-4}	2.407×10^{-4}	2.071×10^{-4}
	256^2	5.201×10^{-5}	4.519×10^{-5}	5.384×10^{-5}
HCR-2 WENO-5	128^2	1.941×10^{-4}	2.170×10^{-4}	1.816×10^{-4}
	256^2	5.161×10^{-5}	4.106×10^{-5}	4.681×10^{-5}

Table 7
Relative ϕ_0 surface area error e_A at different time levels for the three-dimensional coalescing interfaces. Comparison of the solutions computed by the original reinitialization equation (6) and the novel constrained reinitialization equation (15) on different grids. The WENO-5 scheme is used for the spatial discretization.

Reinitialization scheme	Grid	$t = 0.25$	$t = 0.5$	$t = 1$
Original WENO-5	128^2	-2.651×10^{-3}	-4.753×10^{-3}	-8.245×10^{-3}
	256^2	-2.882×10^{-3}	-3.135×10^{-3}	-5.221×10^{-3}
HCR-1 WENO-5	128^2	5.745×10^{-3}	2.231×10^{-3}	1.595×10^{-3}
	256^2	3.282×10^{-4}	1.136×10^{-3}	1.334×10^{-3}
HCR-2 WENO-5	128^2	5.714×10^{-3}	2.069×10^{-3}	1.439×10^{-3}
	256^2	3.752×10^{-4}	1.042×10^{-3}	1.028×10^{-3}

$$\begin{cases} \phi = \frac{\Delta x}{10} & \text{for } \mathbf{x} \in \Omega^+, \\ \phi = 0 & \text{for } \mathbf{x} \in \phi_0, \\ \phi = -\frac{\Delta x}{10} & \text{for } \mathbf{x} \in \Omega^-, \end{cases} \tag{31}$$

resulting in very small level set function gradients at the interface and a zero level set function gradient away from the interface. Note that the original ϕ_0 contour is modified by the initialization (31). For the case of the square interface, this initialization results in a smooth interface as shown in Fig. 14(a) since the square is aligned with the Cartesian grid lines. The curved part of the slotted disk, however, is perturbed as shown in Fig. 14(c). The initial ϕ_0 interfaces are shown in Fig. 14(a) and (c). To compute the signed distance function with respect to these interfaces the reinitialization procedure is used to steepen up the level set function at the respective interfaces and extend this information to the far-field of the domain. Because of the flat profile of the level set function this requires $\mathcal{O}(10^3)$ iterations. For the two cases, the level set function after 2000 iterations of the constrained reinitialization Eq. (15) using the HCR-2 scheme is shown in Fig. 14(b) and (d), respectively. The results for the HCR-1 scheme are alike and omitted for brevity. Fig. 14(b) and (d) qualitatively show that the sharp corners of the square and the small perturbations of the curved part of the slotted disk are retained in the solution even after 2000 iterations of the constrained reinitialization Eq. (15).

A more economic way to generate a signed distance function from a flat level set profile is to use the low-order CR schemes CR-1 or CR-2 [9]. In these schemes, the level set function at the interface is directly computed and used as a boundary condition for the iterative first-order solution of the reinitialization equation. If desired, the converged first-order solution can then be further improved using the HCR schemes.

5.5. Remarks on reinitialization strategies

We end this section with some remarks on reinitialization strategies, that is, we briefly discuss the question: How frequently is the reinitialization to be performed in a level set application? Comparing the test cases presented in Sections 5.1 and 5.2 one can deduce that in terms of the reinitialization strategy, level set applications can be categorized in two groups:

1. The extension velocity is externally prescribed independent of the level set field.
2. The level set extension velocity $\mathbf{f}$ depends on the derivatives of the level set field such as the normal vector $\mathbf{n}$ and/or the curvature $\mathfrak{C}$. Examples of this category include premixed combustion and multiphase flows.

While the reinitialization may only have a minor positive or even an adverse effect on the solution accuracy for problems of the first category, it is particularly important for problems of the second category. This is in agreement with the findings reported in [6,12]. In [6,7], the reinitialization is only used as long as the level set field deviates from the signed distance function by a pre-defined threshold value. A somewhat optimal value of the threshold, however, appears to be highly dependent on the test case. On the other hand, it is shown in [12] that for the oscillating circle test case discussed in Section 5.1, i.e., an application of the second category, the solution quality increases the more often a reinitialization is performed. Hence, for this type of problems a compromise between computational costs and solution accuracy needs to be found. In brief, a general recommendation in terms of the required number of reinitialization steps can hardly be given, and the particular reinitialization strategy depends largely on the type of level set application.

6. Summary

The new constrained reinitialization equation has been introduced in the framework of a novel high-order constrained reinitialization scheme, which is presented in two formulations HCR-1 and HCR-2. This equation is based on the original reinitialization equation and the formulations CR-1 and CR-2 of the constrained reinitialization scheme. It contains a forcing

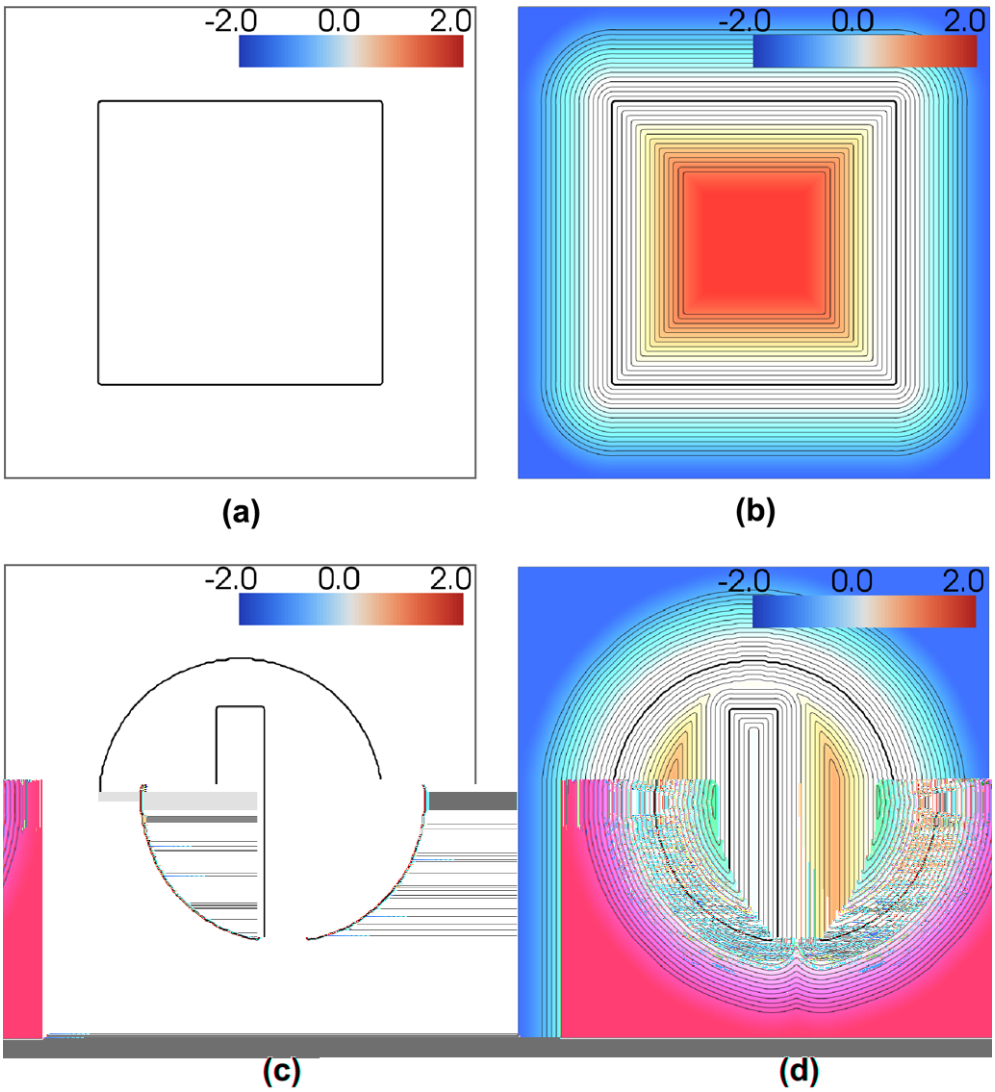

Fig. 14. Computation of the signed distance function using the HCR-2 scheme for a square interface (a and b) and the perturbed Zalesak disk (c and d): (a and c) level set function before the reinitialization; (b and d) level set function after 2000 pseudo-time steps of Eq. (15). The colors correspond to the value of the level set function ϕ, contour lines of which are plotted in intervals of $\Delta\phi = 0.1$ in the range $\phi = \{-1.5, \ldots, 1.5\}$. The ϕ_0 contour is plotted as a thick line.

term which corrects the displacement of the interface during the solution of the reinitialization equation. The general form of the constrained reinitialization equation allows for an arbitrarily high-order discretization.

Numerical experiments have been performed in two-and three-dimensional space using a fifth-order WENO discretization of the original and the constrained reinitialization equation indicating the significantly increased accuracy of the novel HCR scheme. Unlike the standard reinitialization scheme the novel HCR schemes are robust in that a large number of iterations can be performed without compromising the accuracy through the interface displacement. Finally, both formulations HCR-1 and HCR-2 provide similar results, with HCR-2 appearing slightly superior and simpler to implement.

Acknowledgments

This research is part of the Collaborative Research Center SFB 686 which is funded by the German Research Association (Deutsche Forschungsgemeinschaft (DFG)). The support of the DFG is gratefully acknowledged.

References

[1] S. Osher, J. Sethian, Fronts propagating with curvature-dependent speed: algorithms based on Hamilton–Jacobi formulations, J. Comput. Phys. 79 (1988) 12–49.

[2] D. Enright, R. Fedkiw, J. Ferziger, I. Mitchell, A hybrid particle level set method for improved interface capturing, J. Comput. Phys. 183 (2002) 83–116.
[3] M. Sussman, E. Puckett, A coupled level set and volume-of-fluid method for computing 3D and axisymmetric incompressible two-phase flows, J. Comput. Phys. 162 (2000) 301–337.
[4] M. Sussman, E. Fatemi, An efficient, interface-preserving level set redistancing algorithm and its application to interfacial incompressible fluid flow, SIAM J. Sci. Comput. 20 (4) (1999) 1165–1191.
[5] M. Sussman, A. Almgren, J. Bell, P. Colella, L. Howell, M. Welcome, An adaptive level set approach for incompressible two-phase flows, J. Comput. Phys. 148 (1999) 81–124.
[6] P. Gómez, J. Hernández, J. López, On the reinitialization procedure in a narrow-band locally refined level set method for interfacial flows, Int. J. Numer. Meth. Eng. 63 (2005) 1478–1512.
[7] M. Herrmann, A balanced force refined level set grid method for two-phase flows on unstructured flow solver grids, J. Comput. Phys. 227 (2008) 2674–2706.
[8] M. Sussman, P. Smereka, S. Osher, A level set approach for computing solutions to incompressible two-phase flow, J. Comput. Phys. 114 (1994) 146–159.
[9] D. Hartmann, M. Meinke, W. Schröder, Differential equation based constrained reinitialization for level set methods, J. Comput. Phys. 227 (2008) 6821–6845.
[10] D. Peng, B. Merriman, S. Osher, H. Zhao, M. Kang, A PDE-based fast local level set method, J. Comput. Phys. 155 (1999) 410–438.
[11] G. Russo, P. Smereka, A remark on computing distance functions, J. Comput. Phys. 163 (2000) 51–67.
[12] D. Hartmann, M. Meinke, W. Schröder, On accuracy and efficiency of constrained reinitialization, Int. J. Numer. Meth. Fluids (2009). doi:10.1002/fld.2135.
[13] G.-S. Jiang, D. Peng, Weighted ENO schemes for Hamilton–Jacobi equations, SIAM J. Sci. Comput. 21 (2000) 2126–2143.
[14] D. Hartmann, M. Meinke, W. Schröder, Erratum to Differential equation based constrained reinitialization for level set methods, J. Comput. Phys. 227 (2008) 6821–6845 (J. Comput. Phys. 227 (2008) 9696).
[15] R. Nourgaliev, T. Theofanous, High-fidelity interface tracking in compressible flows: unlimited anchored adaptive level set, J. Comput. Phys. 224 (2007) 836–866.
[16] W. Rider, D. Kothe, Reconstructing volume tracking, J. Comput. Phys. 141 (1998) 112–152.
[17] P. Smereka, The numerical approximation of a delta function with application to level set methods, J. Comput. Phys. 211 (2006) 77–90.
[18] S. Zalesak, Fully multidimensional flux-corrected transport algorithms for fluids, J. Comput. Phys. 31 (1979) 335–362.